BIPV/T facades – A new opportunity for integrated collector-storage solar water heaters? Part 1: State-of-the-art, theory and potential

BIPV/T facades – a new opportunity for Integrated Collector-Storage Solar Water Heaters?

Part 1: State-of-the-art, theory and potential

Adrian Pugsley[(a)] (a.pugsley@ulster.ac.uk, +44(0)28 90366264 (corresponding author)
Aggelos Zacharopoulos[(a)] (a.zacharopoulos@ulster.ac.uk) +44(0)28 90368227
Jayanta Deb Mondol[(a)] (jd.mondol@ulster.ac.uk) +44(0)28 90368037
Mervyn Smyth[(a, b)] (m.smyth1@ulster.ac.uk) +44(0)28 90368119

(a) Centre for Sustainable Technologies (www.cst.ulster.ac.uk), School of the Built Environment, Ulster University, Newtownabbey, BT37 0QB, Northern Ireland, UK

(b) SolaForm Ltd (www.solaform.com) c/o Ulster University, Newtownabbey, BT37 0QB, Northern Ireland, UK

Keywords

Integrated Collector-Storage Solar Water Heaters (ICSSWH); Photovoltaic-thermal (PV/T); Thermal diode; building facade; solar collector; heat removal factor

Highlights

- Two-part study proposing an alternative approach to realising BIPV/T facades
- Part 1 reviews theory & potential, Part 2 describes prototype realisation & testing
- Integrated Collector-Storage Solar Water Heater element reduces overheating
- Planar Liquid-Vapour Thermal Diode element reduces overnight heat losses
- Model results show that approach meets conventional performance benchmarks

Abstract

Building Integrated Photovoltaic Thermal (BIPV/T) systems are promising solutions for serving local electricity and heat demands in Net Zero Energy Buildings (NZEB). Despite BIPV/T offering clear energetic and space saving advantages compared to separate BIPV and solar thermal, overheating occurs when no thermal demand exists, resulting in reduced yields, stagnation damage, and excessive fluid pressures. Whilst continuous fluid flows mitigate overheating, corresponding parasitic demands and space requirements are significant (pumps, large storage tanks or heat rejection equipment). This two-part study examines an alternative approach to BIPV/T, addressing overheating by combining BIPV and Integrated Collector-Storage Solar Water Heater (ICSSWH) concepts. Solar heating capabilities of ICSSWH collectors are well established and their overnight heat loss characteristics provide passive

overheating control. BIPV-ICSSWH approaches have yet to be investigated extensively. This paper (Part 1 of 2) reviews state-of-the-art and performance benchmarks in BIPV/T and ICSSWH; proposes new performance metrics enabling fairer comparisons; and develops a heat transfer model for BIPV-ICSSWH façade elements employing Planar Liquid-Vapour Thermal Diodes (PLVTD) to regulate absorber temperatures and heat losses. Multi-day solar thermal collection, photovoltaic generation, and overnight heat retention behaviours are simulated in different climates. The modelling results (experimentally validated in Part 2 of 2) suggests BIPV-PLVTD-ICSSWHs with single transparent covers and $\varsigma \approx 90\%$ PLVTD diodicity achieve $\eta_{T,col} \approx 60\%$ solar thermal efficiency at $N \approx 0.035 m^2K \cdot W^{-1}$, PV/T performance ratio $PR_{T3} \approx 75\%$, and heat loss coefficient $U_{r,sys}A_{sys}/u \approx 20\ W \cdot m^{-3}K^{-1}$. The novel BIPV-PLVTD-ICSSWH approach can reduce maximum stagnation by 20°C compared to conventional BIPV/T and therefore support NZEB realisation during global efforts to tackle the climate crisis.

Graphical abstract

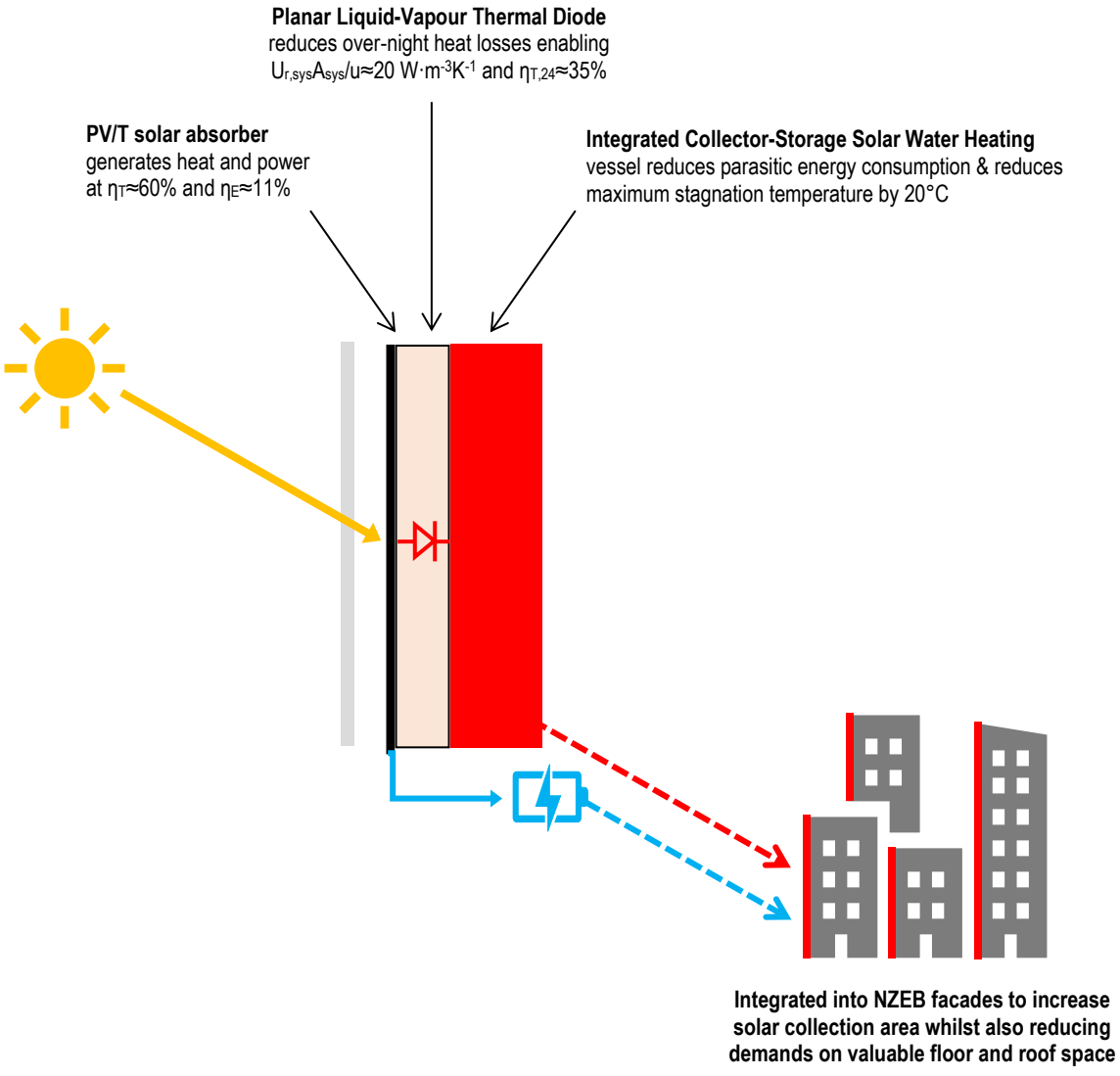

1 Introduction

Net-Zero Energy Buildings (NZEB) are increasingly being designed with Building Integrated Photovoltaics (BIPV) to generate electricity and Building Integrated Solar Thermal Systems (BISTS) to supply domestic hot water and thermal energy to contribute towards space heating demands (COST, 2015). Approximately one-third of global final energy consumption (125 of 400EJ annually) can be attributed to residential and service sector buildings (IEA, 2018; IEA/UN, 2018) where it is primarily used for space heating & cooling (40%) and domestic hot water production (20%). Buildings are correspondingly responsible for ~39% of global CO_2 emissions which need to be radically and rapidly cut in order to mitigate the climate crisis. For residential and commercial buildings in a variety of climates, BISTS can provide between 10% and 90% of space heating and domestic hot water energy demands (Smyth et al., 2006; Li et al., 2013; Drosou et al., 2014; O'Hegarty et al., 2014; Good et al., 2015; Mehdaoui et al., 2019; Beausoleil-Morrison et al., 2019; Billardo et al., 2019) and BIPV can cover similarly large proportions of building electrical loads (Good et al., 2015; Sorgato et al. 2018; Belussi, 2019; Li et al., 2019). Mismatches between energy demands and solar availability (instantaneously, diurnally and over inter-seasonal timescales) mean that thermal energy storage is an essential part of most BISTS and is crucial for achievement of a high solar fraction. Electrical energy storage is likewise crucial for high solar fraction BIPV systems and can be implemented in the form of batteries or as "virtual storage" via an import-export connection to the grid, perhaps in combination with load scheduling (Kats and Seal, 2012). Integrated Collector-Storage Solar Water Heater (ICSSWH) concepts have potential to reduce the costs of BISTS and to minimise loss of valuable floor space associated with conventional solar hot water storage. Very few authors (Krauter, 2004; Ziapour et al., 2014; Pugsley et al., 2016) have considered the potential for combining PV and ICSSWH concepts, integrating ICSSWHs into building facades (Smyth et al., 2019; Harmim et al., 2019), or using them as a thermal source for heat pumps (Pugsley et al., 2017). The present work examines the synergy of combining PV and ICSSWH concepts in the BIPV and BISTS context and explores potential benefits of introducing Planar Liquid-Vapour Thermal Diodes (PLVTDs) to improve PV-thermal heat transfer and reduce overnight heat losses.

Traditionally, solar thermal and photovoltaic collectors have been applied as bolt-on elements to building envelopes, usually fixed to roofs and tilted towards the equator at the latitude angle to maximise annual insolation, or in some cases fixed to facades. These building applied collectors compete for available space and can adversely affect the visual aesthetics of building exteriors. Table 1 summarises insolation and average

irradiance levels for three contrasting climate locations (Belfast, UK; Rome, Italy; Riyadh, Saudi Arabia) at different latitudes based on 22 years of extra-terrestrial solar radiation measurements and earth surface satellite imagery (NASA, 2019; Stackhouse et al., 2018). Large seasonal and locational variations are apparent for horizontal ($100<G_{avg}<600$ W/m^2 and $3<H_{24}<27$ MJ/m^2), latitude tilted ($200<G_{avg}<600$ W/m^2 and $5<H_{24}<24$ MJ/m^2) and sun tracking surfaces ($200<G<800$ W/m^2 and $6<H_{24}<37$ MJ/m^2). Equator-facing vertical surfaces consistently receive $200<G_{avg}<500$ W/m^2 and $4<H_{24}<14$ MJ/m^2 for all three locations which represents a much more seasonally stable resource, albeit of generally lower intensity. The daily insolation received by a vertically oriented equator-facing surface corresponds to 60-75% of the maximum available (relative to a sun-tracking surface) in winter and 19-46% of the maximum available energy in summer. It should be noted that much higher instantaneous irradiances ($G_{inst}\approx1000$ W/m^2, occasionally higher due to cloud reflections) will occur on clear sunny days at times when the sun is aligned normal to the collector plane.

Building Integrated Photovoltaic-Thermal (BIPV/T) systems combine solar electricity and thermal energy (hot air and/or water) generation into the building envelope. The collectors form an integral part of the architecture to make aesthetically pleasing and efficient use of all available insolated building envelope surfaces. This becomes increasingly important for NZEBs, especially where there is a high ratio of energy demand to envelope surface area, and in particular to the case of relatively tall buildings (Saretta et al., 2020) where roof space for solar collectors (and likewise land area for ground source heat collection) is inherently limited. Façade integrated BIPV/T is a good option in higher latitude locations (such as Belfast) where significant energy is required for heating and lighting in winter when the solar altitude is low and vertical surfaces receive more insolation than horizontal surfaces (see Table 1). Despite offering clear energetic advantages when suitable thermal demands exist, PV/T collectors suffer similar stagnation and overheating problems as closed-back BIPV systems (ie reduced electrical yields and eventual delamination damage) and conventional solar flat plate solar water heaters (ie over-pressurisation, denaturing of heat transfer fluids, damage to selective coatings, melting of polymeric components) when no thermal demands exist. This can be avoided by ensuring continuous fluid flows on hot sunny days but the corresponding parasitic energy requirements (eg for pumps and/or heat rejection fans) typically far exceed the modest gains in electrical yields and the ancillary equipment (large thermal stores and/or heat rejectors) occupy valuable floor space.

Table 1 – Comparison of solar radiation levels on horizontal, vertical, tilted, and sun-tracking surfaces at different latitudes

		Cool, wet and cloudy climate	Warm and sunny climate	Hot, dry and very sunny climate
Location (Latitude, Longitude)		Belfast, UK (54.6N, 5.9W)	Rome, Italy (41.9N, 12.5E)	Riyadh, Saudi Arabia (24.6N, 46.7E)
Annual global horizontal insolation [(a)] (H_{h365}, MJ/m^2)		3247	6073	7495
Summertime [(a)] **average daily insolation** (H_{24}, MJ/m^2)	Horizontal surface	15.3	25.8	26.6
	Sun tracking surface	20.4	37.3	35.8
	Latitude tilted surface	13.8	23.8	24.3
	Vertical surface	9.4	11.5	6.9
	Daylight hours duration (t_{day}, hours)	16.2	14.6	13.4
Wintertime [(a)] **average daily insolation** (H_{24}, MJ/m^2)	Horizontal surface	2.7	7.7	14.2
	Sun tracking surface	5.9	16.8	23.7
	Latitude tilted surface	4.7	13.1	17.6
	Vertical surface	4.4	12.4	14.3
	Daylight hours duration (t_{day}, hours)	8.4	9.8	10.9
Summertime [(b)] **typical irradiance** (G_{avg}, W/m^2)	Horizontal surface [(c)]	279	527	596
	Sun tracking surface [(c)]	373	762	802
	Latitude tilted surface [(d)]	270	525	592
	Vertical surface [(e)]	**215**	**292**	**191**
Wintertime [(b)] **typical irradiance** (G_{avg}, W/m^2)	Horizontal surface [(c)]	101	243	398
	Sun tracking surface [(c)]	221	530	665
	Latitude tilted surface [(d)]	204	467	549
	Vertical surface [(e)]	**194**	**469**	**486**

Table notes:

a) Data from NASA (2019) based on averages for the summer months May, June, July and August and winter months November, December, January and February. Values for sun tracking collectors are based on total diffuse plus direct radiation.

b) Based on average daily insolation level divided by the estimated number of "useful" daylight hours.

c) The number of "useful" daylight hours for a sun tracking surface is taken to be 1 hour less than the total number of daylight hours to account for the fact that the sun is partially obscured by the horizon at dawn and dusk.

d) The number of "useful" daylight hours for horizontal and equator-facing latitude-tilted surfaces is taken as 2 hours less than the total number of daylight hours. This is to reflect the fact that the sun is incident at grazing angles (<15° relative to the collector plane) during the first and last hours of the day, which results in these surfaces receiving <25% of the available direct beam irradiance.

e) The number of "useful" daylight hours for equator-facing vertical surfaces is taken as 75% of the total number of daylight hours to account for dawn and dusk grazing incidence angles (as explained in Note "d") plus additional grazing incidence angles which occur near solar noon at low latitude locations during summer.

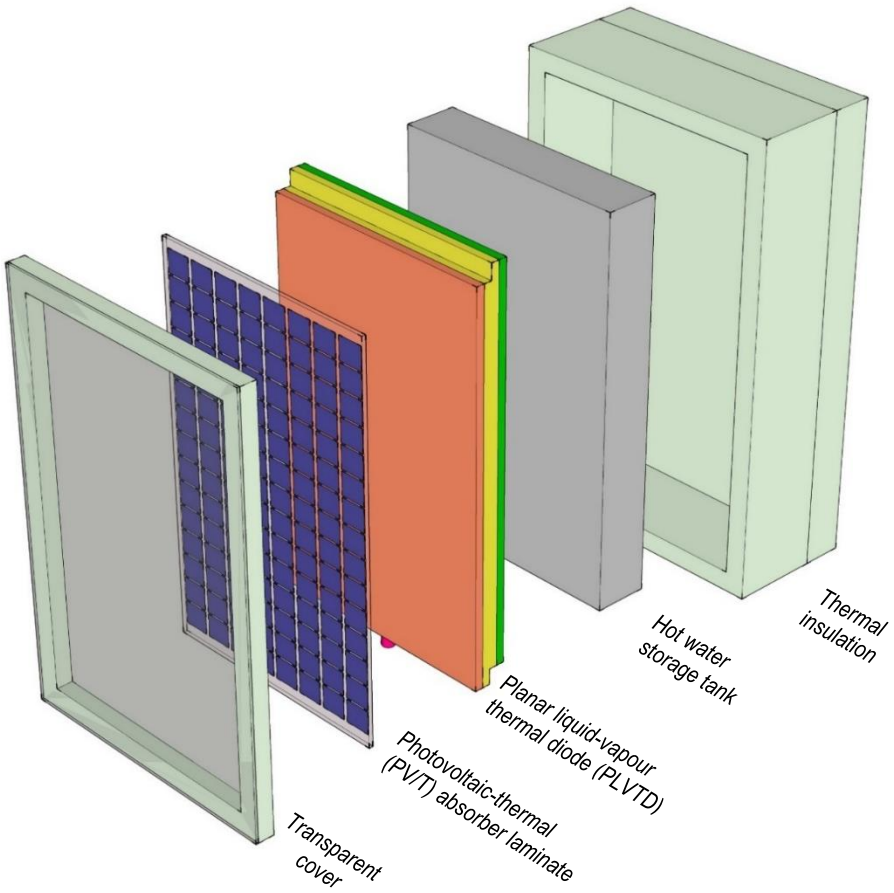

Figure 1: Key components of the BIPV-PLVTD-ICSSWH concept

Integrated Collector-Storage Solar Water Heaters (ICSSWH) are an alternative to conventional flat plate or evacuated tube collector solar water heating systems. Whilst ICSSWH systems suffer significant overnight heat losses (eg unavailability of stored heat for morning bathing etc) they offer a number of advantages in respect of cost, space, and inherent passive protection from overheating. Development of the novel BIPV-PLVTD-ICSSWH concept proposed in this two-part study has the potential to overcome key problems associated with the individual technologies (namely, BIPV/T overheating during stagnation, and ICSSWH overnight heat losses) and to realise new synergies. An exploded diagram illustrating the component parts of a BIPV-PLVTD-ICSSHW collector is shown in Figure 1. The present paper (Part 1 of 2) introduces the BIPV-PLVTD-ICSSWH concept; reviews the fundamental operating principles of PV/T, ICSSWH and PLVTD components; and establishes state-of-the-art performance benchmarks. A new heat loss performance metric ($U_{r,sys}A_{sys}/u$ with units $W \cdot m^{-3} \cdot K^{-1}$) is proposed to enable ICSSWHs of differing sizes and shapes to be compared more fairly. New thermal and electrical performance metrics (diurnal thermal efficiency $\eta_{T,24}$ and PV/T performance ratio PR_{T3}) are also proposed to facilitate better comparisons

between different technologies. An energetic model of the BIPV-PLVTD-ICSSWH concept is presented and some key theoretical considerations concerning heat removal factors and thermal diodicity are discussed. The energy model has been used to predict temperatures, solar thermal collection, photovoltaic generation, and overnight heat retention behaviours over multi-day periods in a variety of climates. Modelling results have been compared with appropriate benchmarks to highlight the potential benefits of the BIPV-PLVTD-ICSSWH concept in the context of applications in NZEB facades. The concluding part of the study is presented in a separate paper (Part 2 of 2) which describes realisation and laboratory testing of a prototype to demonstrate operation and validate the theoretical model.

2 State-of-the-art in relevant technologies

2.1 Photovoltaic-thermal (PV/T) systems

The concept of combining PV and thermal absorbers into a single collector initially arose from a need to remove unwanted heat from early PV modules (especially those incorporating concentrating reflectors) whose electrical efficiency was compromised by high temperatures. The first PV/T collectors were designed to use this "waste" heat for residential water and air heating applications. Zondag (2008) gives a comprehensive review of 30 years of flat plate PV/T collector development and more recent reviews are given by Michael et al. (2015); Besheer et al. (2016) and Sultan & Efzan (2018), amongst others. Whilst popularity of PV systems has sky-rocketed in recent years owing to rapidly declining costs, PV/T systems have failed to achieve commercial success. Recent academic advances in PV/T collector development have explored the use of nanofluids to improve heat transfer and nanomaterials for phase change thermal storage or optical filtering (Abdelrazik et al., 2018; Das et al., 2018). Recent advances in system-level approaches, applications, and economics of BIPV/T (Buonomano et al., 2016; Yang & Athienitis, 2016; Barone et al., 2019) include studies on heat pump integration (Good et al., 2015; Calise et al., 2016; Qu et al., 2016) and the multifunction façade context (Li et al., 2019; Tian et al., 2019).

2.2 Electrical behaviour of PV/T systems

Electrical efficiencies of PV/T collectors are typically 5 to 15% depending on PV cell material type and heat delivery temperature. The main drivers of electrical efficiency (assuming no shading) are the inherent PV cell efficiency characteristics; cell operating temperature; and optical losses. Individual PV cells each nominally produce ~0.5V,

although voltage reduces with increasing temperature and tends towards zero under low irradiance or short circuit conditions. Current flows depend upon PV cell material type and are proportional to area and incident irradiance level; inversely proportional to applied electrical load resistance (tending to zero under open circuit conditions); and typically increase slightly with increasing cell temperature. Cells connected together in series all operate at the same current, while cells connected in parallel all operate at the same voltage. Temperature gradients sometimes exist over PV/T absorber surfaces causing cells to operate at different maximum power points. Operating point voltage differences caused by temperature non-uniformities can significantly reduce electrical efficiency if cells are connected in parallel but generally have minimal effect on series connected cells. Monocrystalline (mc-si) and polycrystalline (pc-si) silicon PV cells, and amorphous silicon (a-si), Cadmium Telluride (CdTe) and Copper Indium Gallium Selenide (CIGS) thin film cells have all successfully been used for PV/T. Crystalline silicon typically offers high efficiency ($15<\eta_E<18\%$) at low temperatures but pronounced reductions occur with increasing temperature. Lower efficiencies ($6<\eta_E<12\%$) are typical for thin film cell types. Multijunction cells, formed of several layers of different PV materials with different band gaps, have the highest known photovoltaic efficiencies but are expensive and typically only used for spacecraft applications. Inclusion of transparent covers over PV/T absorbers significantly reduces heat loss but correspondingly increases optical losses and hence reduces electrical efficiency. Experimental work by Guarracino et al. (2019) found that transparent covers can significantly reduce electrical efficiency, especially at oblique solar incidence angles when refection losses are typically more significant than cell temperature effects. Zondag (2008) suggests uncovered BIPV/T façade electrical efficiencies are commonly enhanced by ~10% compared to non-ventilated BIPV due to beneficial heat removal but can be compromised by ~10% compared to conventional naturally ventilated roof-mounted PV modules if heat delivery temperatures are high (similar findings are reported by Fuentes et al., 2018). Net electrical yields from BIPV/T systems can be lower than those from BIPV owing to the parasitic electricity consumption by pumps and fans facilitating heat removal. Parasitic consumption increases when buildings have no significant heat demand (eg no space heating required in summer and relatively low hot water usage) and waste heat rejection equipment becomes necessary to prevent overheating damage caused by stagnation (delamination, excess fluid pressures, etc).

Cells and modules are commonly characterized with reference to Standard Test Conditions (STC at $G=1000$ W/m^2 irradiance with spectrum AM1.5 and $T_0=25$°C cell

temperature) using performance metrics derived from current-voltage curves. Key metrics (defined in Equations 1 to 4) include short circuit current (I_{sc}), open circuit voltage (V_{oc}), electrical power delivered at the maximum power point ($q_{E,mpp}$), fill factor (FF), voltage-temperature coefficient ($K_{V:T}$), current-temperature coefficient ($K_{I:T}$) and voltage-irradiance coefficient $K_{V:G}$. Performance deviates from the ideal current-voltage curve (FF_{ideal} = 1) with increasing irradiance and increasing temperature such that typical real values are $0.75<FF_{STC}<0.85$ and $K_{V:T}$ = -0.45%/K for c-si and $0.5<FF_{STC}<0.7$ and $K_{V:T}$= -0.25%/K for thin film (DGS, 2008). Current-temperature coefficients ($K_{I:T}$) and are usually positive but an order of magnitude smaller than $K_{V:T}$. According to Santbergen et al. (2010) non-linear voltage-irradiance coefficient values are typically $K_{V:G}$≈100% for irradiances of primary interest ($400<G<1200$ W·m^{-2}), $K_{V:G}$≈80% for cloudy conditions (G=100 W·m^{-2}) and $K_{V:G}$<50% for very low irradiances (G<50 W·m^{-2}).

The electrical output of a conventional PV module operating under realistic conditions deviates significantly from that occurring under STC owing to a variety of cell temperature and irradiance effects. Cell temperatures (T_0) are determined by the ambient temperature (T_a) and incident irradiance level (G) as well as module mounting arrangements and local wind speed effects. Irradiance incident on the PV cell surface is determined by the prevailing irradiance level and spectrum (which are functions of latitude, time of day, module mounting angle, and local weather conditions) as well as optical losses associated with cell coverings (eg cover glass, cell encapsulation materials, front-of-cell electrical contacts etc). Deviations relative to STC are further pronounced in the case of PV/T modules owing to the influence of the fluid temperature (T_3) upon the cell temperature (T_0) and because transparent covers required to reduce heat loss inherently reduce the effective transmissivity (τ). A sensible approach to the characterization of PV/T module electrical performance is therefore to define a Performance Ratio comparing the device's maximum electrical power output ($q_{E,mpp,T3}$) at operating fluid temperature (T_3) relative to a chosen reference value. Santbergen et al. (2010) use the standard maximum power output (q_{STC}) as the reference value (PR_{STC} as defined by Equation 5). We propose an alternative (PR_{T3} as defined by Equation 6) which takes the reference value as being the power output of an ideal PV/T module with perfect optical (τ=1) and heat transfer characteristics (F=1 so that $T_0=T_3$) and full coverage of the absorber by PV cells ($A_0=A_1$). Based on work of other authors (notably Zondag et al., 2003; Santbergen et al., 2010 and Guarracino et al., 2019) suitable benchmark values are PR_{T3}=85% and PR_{T3}=75% for uncovered and covered collectors respectively.

$$q_{E,mpp} = I_{mpp} \cdot V_{mpp} = FF \cdot I_{sc} \cdot V_{oc} \quad \text{Equation 1}$$

$$K_{V:T} = \frac{V_{oc,T_0} - V_{oc,STC}}{V_{oc,STC}\,(T_0 - 25)} \quad \text{Equation 2}$$

$$K_{I:T} = \frac{I_{sc,T_0} - I_{sc,STC}}{I_{sc,STC}\,(T_0 - 25)} \quad \text{Equation 3}$$

$$K_{V:G} = \frac{V_{oc,G}}{V_{oc,STC}} \quad \text{Equation 4}$$

$$PR_{STC} = \frac{Electrical\ efficiency\ of\ PVT\ operating\ at\ T_3}{Electrical\ efficiency\ of\ single\ cell\ operating\ at\ STC} = \frac{\eta_{E,mpp,T_3}}{\eta_{STC}} = \frac{q_{E,mpp,T3}(G \cdot A_1)^{-1}}{q_{STC}(G_{STC} \cdot A_0)^{-1}} \quad \text{Equation 5}$$

$$PR_{T3} = \frac{Electrical\ efficiency\ of\ PVT\ operating\ at\ T_3}{Electrical\ efficiency\ of\ single\ cell\ operating\ at\ T_3} = \frac{PR_{STC}}{2-(1-[T_3-25]K_{V:T}) \cdot (1-[T_3-25]K_{I:T})} \quad \text{Equation 6}$$

2.3 Thermal behaviour of PV/T systems

Solar thermal efficiencies of PV/T collectors are typically $60<\eta_T<80\%$ when working fluid and ambient temperatures are equal (zero loss condition) but commonly $\eta_T<30\%$ for collectors producing domestic hot water in cool climates. Cell type and packing factor; front-of-cell electrical contacts or transparent conductors; absorber substrate characteristics; and encapsulation material properties, together determine the optical properties and heat transfer characteristics of PV/T absorbers. Solar thermal efficiencies of PV/T absorbers are generally lower than those of dedicated solar heat collectors because absorption coefficients ($0.7<\alpha<0.9$) and emissivities ($0.2<\varepsilon<0.6$ bare or $0.7<\varepsilon<0.9$ encapsulated) of PV cells are inferior to those achieved by solar selective coatings ($\alpha\approx0.95$ and $\varepsilon\approx0.1$). Thermal efficiencies are also inherently reduced because a proportion of the input solar energy is converted to electricity when a suitable load is connected (Guarracino et al., 2019). High emissivities of PV cells and encapsulation materials increases radiative heat losses which become particularly significant at high heat delivery temperatures. Typical PV/T collector constructions are discussed in detail by Santbergen et al. (2010) and Dupeyrat et al. (2011). Most liquid-heating PV/T collectors take the form of individual PV cells or whole module laminates glued or bonded to conventional metal solar thermal absorbers (eg sheet-and-tube, flow channel, or roll-bond types). High thermal conductance through bonding layers joining PV cells to absorber substrates is required to minimise absorber temperatures, minimise heat losses, and maximise solar thermal efficiency. Likewise, convective heat transfer between absorber substrates and working fluids should be maximized. Zondag (2008) discusses PV/T collectors featuring overall conductances in the range 40 to

250 $W \cdot m^{-2}K^{-1}$ with the poorest example of heat transfer occurring in a collector featuring a 5mm silicone bonding layer where cell-to-fluid temperature difference was 12°C corresponding to >10% reduction in thermal output and ~5% reduction in electrical yield. Dupeyrat et al. (2011) fabricated a high efficiency collector with 0.5mm thick Ethylene-Vinyl Acetate bonding layer achieving 700 $W \cdot m^{-2}K^{-1}$ between PV cells and a 1.2mm roll-bond aluminium thermal absorber. Fragile PV cells must be protected against damaging mechanical forces (eg torsions during handling, wind loads, and impacts from hail or vandalism); protected against water ingress; and electrically isolated from metal substrates. External protection usually takes the form of a glass or transparent polymer layer bonded to the front side of the PV cells. This can be supplemented by one or more tertiary transparent covers to reduce heat loss in cases where high delivery temperatures or operation in cold and windy climates is required (ie heat delivered at >20°C higher than ambient). Like conventional solar thermal collectors, PV/T must be protected against high stagnation temperatures (especially when fitted with tertiary transparent covers) and withstand thermal shocks caused by rapid changes in climatic conditions or fluid flow transients (eg cold water flowing into hot collectors). Damage can occur due to high fluid pressures; differential thermal expansion stresses; melting and UV light degradation of polymeric component materials. Stagnation damage prevention requires continuous operation of fluid circulation systems during hot and sunny periods and heat rejection systems may be required when thermal demands are low or intermittent.

2.4 Integrated Collector-Storage Solar Water Heaters

Solar water heating systems typically have three main components: the collector, the heat transfer system, and the storage vessel. Storage vessels in conventional pumped solar water heating systems tend to be bulky and consume valuable floor space. In hot climates, thermosiphon solar water heaters with close-coupled storage tanks are popular owing to their passive operation, simple installation, externally located storage tank, and relatively low cost. Integrated Collector-Storage Solar Water Heaters (ICSSWH) combine the solar absorber and the thermal storage tank into a single unit to save floor space within the building and to reduce the amount of pumping energy required. They are usually passive devices in which part of the storage tank envelope is used as a solar absorber. This minimises system size and quantity of material required for manufacturing, leading to lower unit costs (Tripanagnostopoulos & Souliotis, 2006), less embodied energy, and greater space efficiency. The greatest drawback of ICSSWHs and close-coupled thermosiphon solar water heaters is that a

large area of storage vessel surface is inherently exposed to the outdoor environment and thus susceptible to heat loss, especially in cold and windy climates. Smyth et al. (2006) provides a comprehensive review from a technical perspective and traces development history back to the 1800s. A more recent review by Singh et al. (2016) attempts to categorise designs according to whether they are non-concentrating (eg flat plate or tank box systems), concentrating (eg compound parabolic) or employing phase change materials. The working principle of an ICSSWH is shown in Figure 2 and the key components and design considerations are:

- **Collector inclination and orientation** affects diurnal and seasonal variation of solar radiation incident on absorber surfaces and also affects natural convection and storage tank stratification.
- **Transparent covers** minimize convective (and some radiative) absorber heat losses and are essential for ICSSWH collectors designed to produce domestic hot water or to operate in cold and windy climates.
- **Storage tank size, shape, & configuration** affect collection and retention efficiencies, stratification and achievable temperature. Tanks are usually heavily insulated on their non-absorbing sides to reduce heat loss.
- **Fabrication material choices** are the primary factor determining cost but also affect solar absorption and heat transfer characteristics (desired solar gains and unwanted losses), robustness and longevity.

Original academic works on ICSSWH technologies over the last decade have examined tank temperature stratification and draw-off mixing effects (Garnier et al., 2009; Borello et al., 2012); use of thermal diodes and concentrating reflectors to reduce heat loss (Souliotis et al., 2011&2017; Smyth et al., 2015a&b, 2017, 2018, 2019; Muhumuza et al., 2019a&b and 2020); and use of phase-change thermal storage materials and heat pipes (Tarhan et al., 2006; Eames & Griffiths, 2006; Chaabane, 2014; Bilardo et al., 2019). Studies by Krauter (2004) and Ziapour et al. (2014) examined the performance (respectively through experimental and simulation work) of novel PV-ICSSWH devices and identified a dearth of published work on similar concepts. Facade integration of PV-ICSSWH units (Pugsley et al., 2016 & 2017; Smyth et al., 2019) has potential to increase available solar collection area, save floor space, reduce parasitic pumping energy requirements, and reduce material costs, but presents a number of practical challenges such as imposed structural loadings and maintenance access arrangements (considered in more detail in Part 2 of 2).

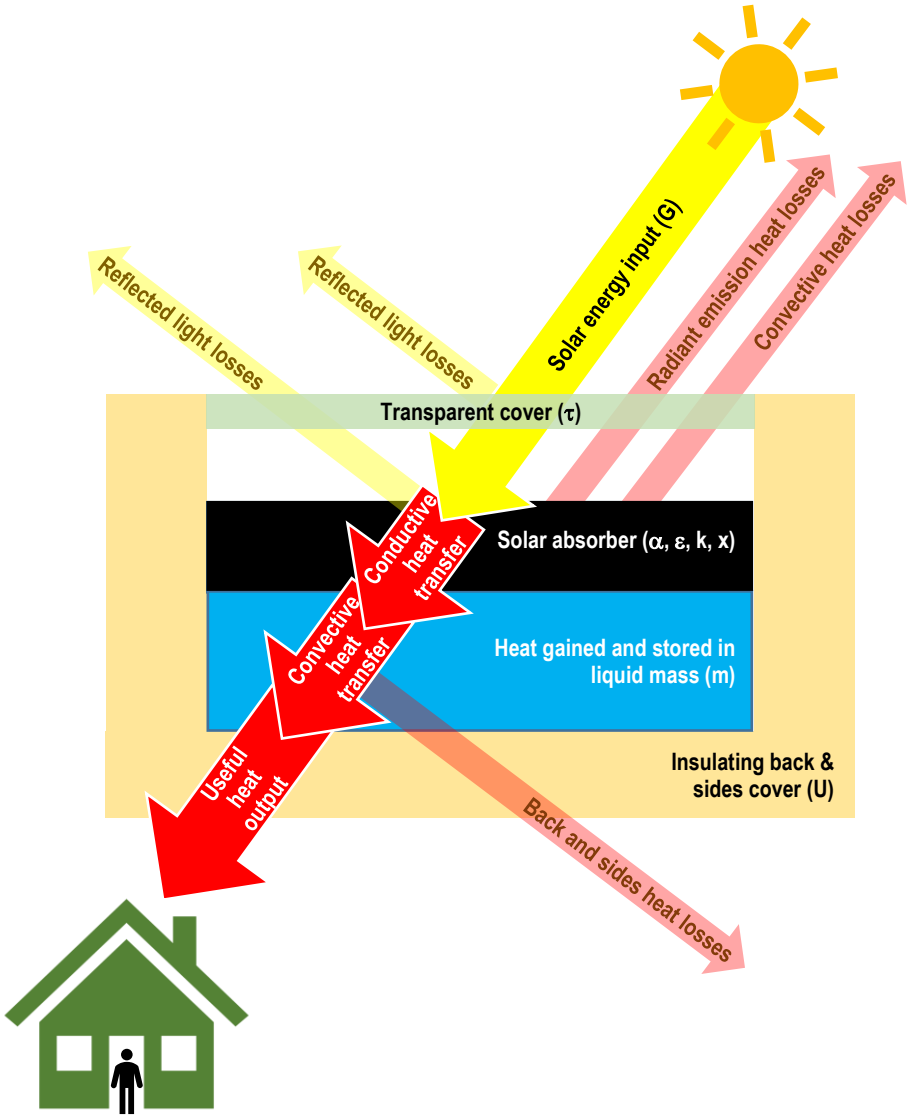

Figure 2: Energy conversion and loss mechanisms in ICSSWH

Almost all ICSSWH collectors feature some form of transparent cover because overnight tank heat losses from uncovered absorbers would result in unacceptably low morning-time tank temperatures. Solutions such as double covers, thermal diodes, or heat pipes need to be considered for ICSSWH systems designed to produce domestic hot water when operating in cold and windy climates. The volume-to-absorber area ratio (u/A) is an important consideration in ICSSWH design as this determines the rate at which the tank gains heat from the incident sunlight during collection periods and also the rate at which heat is lost from the absorber to the ambient environment during retention periods (cloudy or overnight). Storage tank shape can significantly affect the solar collection and heat retention performances (owing to its influence on absorber orientation and exposure; thermal stratification; and overall heat loss coefficients) as well as physical robustness and aesthetics. In particular, tall tanks tend to promote stratification (which maximises potential heat delivery temperatures); triangular and

trapezoidal shapes enable inherent tilting of absorber surfaces (to align with the sun); whilst cylindrical tanks offer inherent passive single-axis solar tracking and tend to be more robust than cubic tanks. Tank envelopes must support the weight of water contained within them and be able to withstand thermal expansion pressures (sealed units/systems) and any externally imposed hydraulic pressures (from mains water or raised header feed tanks). Tanks must be insulated to minimise heat loss from the back and sides (those not used to absorb solar heat) but the insulation thickness can add significantly to overall size. Smyth et al. (2006) and Singh et al. (2016) cite numerous ICSSWH collector examples featuring single or multiple cylindrical, cuboid, triangular, trapezoidal and pyramid tanks with volume-to-absorber area ratios in the range $0.05<u/A<0.3$ m^3/m^2 with 0.1 m^3/m^2 being a typical tank size. Small volumes of stored water cause large diurnal temperature fluctuations in solar heating systems. Larger volumes reduce fluctuation magnitudes thereby reducing summertime overheating and wintertime freezing risks, but the resulting reduced maximum temperatures can increase legionella risks. Schmidt & Goetzberger (1990) suggest $u/A>0.07$ m^3/m^2 for Northern European climates to reduce freeze risks. Amerongen et al. (2013) suggests limiting criteria of $u/A<0.03$ m^3/m^2 and $u/A<0.06$ m^3/m^2 for northern and southern European climates respectively in respect of controlling legionella risk in direct-flow solar water heating systems. Using ICSSWH principles in the context of BIPV/T presents an opportunity to prevent damagingly high stagnation temperatures without the need for heat rejection equipment and offers significant potential benefits in terms of reducing parasitic energy consumption for fluid pumping. Such systems should be designed as indirect-flow types which employ heat exchangers to mitigate legionella risk.

2.5 Solar thermal collection and heat retention behaviour

The thermal power output (q_T) of solar thermal collectors is conventionally represented in the Hottel-Whillier-Bliss form (Equation 7) and presented in the form of efficiency curves (see Figure 3) where the x-axis is the solar thermal condition (N according to Equation 8) and the y-axis is the instantaneous solar thermal collection efficiency (η_T according to Equation 9). On such plots, the y-axis intercept indicates maximum solar thermal efficiency under zero heat loss conditions ($\eta_T = F \cdot \tau \cdot \alpha$ where T_3-T_a=0); the line gradient ($F \cdot U_L$) represents the overall heat loss coefficient referenced to the absorber area (A_1); and the x-axis intercept indicates the stagnation condition (maximum achievable temperature for a given N when $\eta_T \rightarrow 0$ and $T_3 = T_1$). The y-axis intercept is sometimes referred to as the "optical efficiency" because many conventional solar thermal collectors achieve near perfect absorber-to-fluid heat transfer under these conditions ($F>0.95$) and overall efficiency is determined by the transmission-

absorption product $(\tau \cdot \alpha)$. Heat removal factor (F) describes the effectiveness of absorber-to-tank heat transfer which can be expressed according to Equation 10. Production of electricity reduces the amount of heat available for transfer into the tank thus Equation 10 remains valid for the hypothetical scenario of 100% electrical efficiency where $q_E=G \cdot A_1$ which would result in F=0.

$$q_T = F \cdot G \cdot A_1 \left([\tau \cdot \alpha] - \left[U_L \frac{T_3 - T_a}{G} \right] \right) \quad \text{Equation 7}$$

$$N = \frac{T_3 - T_a}{G} \quad \text{Equation 8}$$

$$\eta_T = \frac{q_T}{G \cdot A_1} \quad \text{Equation 9}$$

$$F = \frac{Heat\ transferred}{Maximum\ heat\ available} = \frac{q_T}{[\tau \cdot \alpha - \eta_E] \cdot G \cdot A_1} \quad \text{Equation 10}$$

$$-q_T = U_{r,sys}\, A_{r,sys}\, (T_3 - T_a) \quad \text{Equation 11}$$

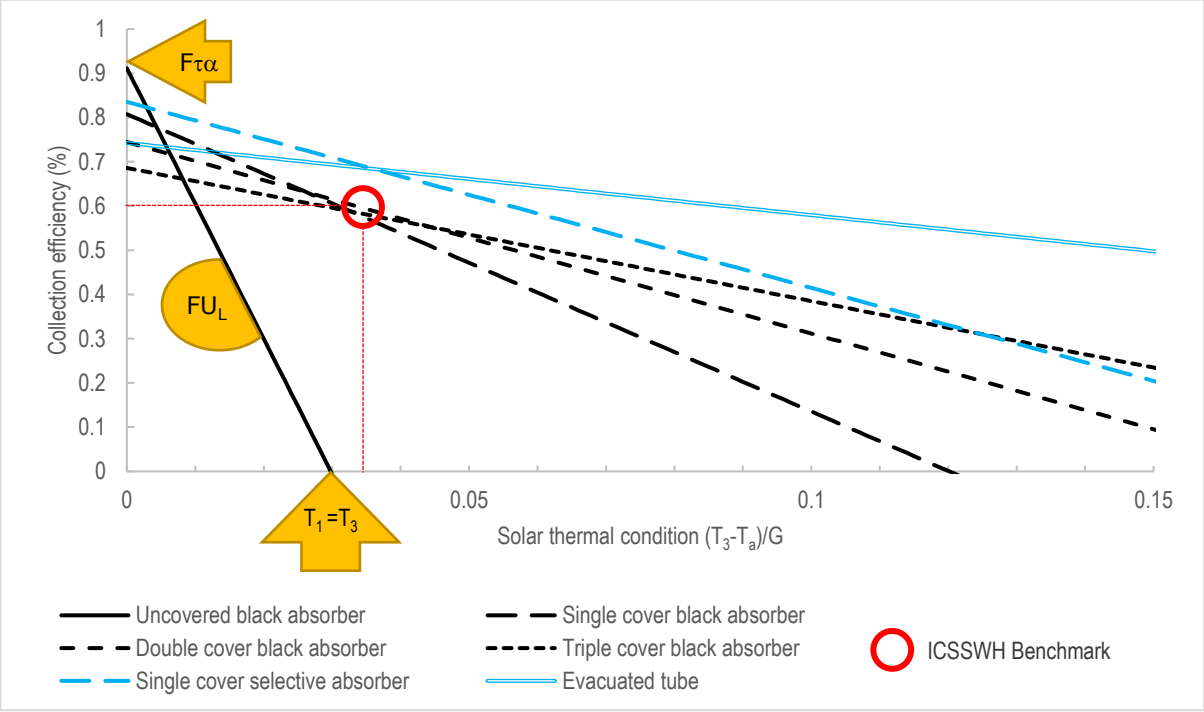

Figure 3: Typical solar collector performance characteristics (at 2m/s wind speed)

Equations 7-10 are only relevant when the collector is illuminated (G>0). When the ICSSWH is in darkness, the total heat loss ($-q_T$) is determined by the overall heat loss coefficient (U_{sys}) referenced to the overall envelope heat loss area (A_{sys}) and the temperature difference between the tank and the ambient (T_3-T_a) as expressed by Equation 11. The key difference between the collection and retention heat loss

coefficients is that U_{sys} describes the total heat loss from the storage tank assuming that it emanates from the whole envelope (A_{sys}) whereas U_L describes the total heat loss from the storage tank assuming that it emanates from the absorber (A_1) which is separated from the storage tank by heat removal factor F. The effective heat loss area can be taken as approximately equal to the absorber area ($A_{sys}\approx A_1$) if the storage tank and sides of the collector are highly insulated or approximately equal to the whole envelope area ($A_{sys}\approx A_1+A_{3i}$) if the insulation of the storage tank and sides has similar performance characteristics as the transparent cover. It is difficult to determine a sensible value for A_{sys} in other less definite cases.

In the case of conventional solar thermal collectors where heat is extracted and delivered by a continuous fluid flow, the thermal power gain can be determined through steady state testing based upon the mass flow rate, specific heat capacity, and inlet-to-outlet temperature difference ($q_T=m\cdot c_p\cdot\Delta T_{out\text{-}in}$). However, in the case of ICSSWH devices, there is commonly no fluid flow during solar collection periods and thus steady state conditions rarely occur (except in the very unusual case where a concurrent heat demand exactly matches solar heat collection). Instead, the thermal power gained by an ICSSWH is usually determined using either quasi steady-state or whole-day testing based upon the rate of temperature rise of the stored thermal mass ($q_T=M\cdot c_p\cdot\Delta T_3/t_{col}$). Equation 12 defines the total insolation (H_{col}) during the collection period (t_{col}) to enable determination of daily average solar thermal efficiency ($\eta_{T,col}$) according to Equation 13. The ability of an ICSSWH collector to retain stored heat for a period of time (t_{ret}) when no solar resource is available (eg at night when G≈0) can be quantified in terms of heat retention efficiency ($\eta_{T,ret}$ according to Equation 14) which is defined as the ratio of thermal energy in the tank at the end of the retention period ($t=t_{col}+t_{ret}$) divided by the thermal energy in the tank at the start of the retention period ($t=t_{col}$). Collection periods are chosen to represent specific latitudinal and seasonal circumstances but are commonly taken as 6, 8 or 12 hrs (t_{col}=21600, 28800 or 43200s) with corresponding retention periods of 18, 16 or 12 hrs (t_{ret}=64800, 57600 or 43200s). Energy contained in the tank at a given time ($Q_{T[t]}$) is determined by the product of its heat capacity ($M\cdot c_p$) and temperature ($T_{3[t]}$) normalised to respective ambient temperatures at the end of the preceding collection period ($T_{a[t_{col}]}$) and averaged throughout the retention period ($\tilde{T}_{a[t_{ret}]}$). Retention efficiency can be used to determine an overall reverse mode heat transfer coefficient ($U_{r,sys}A_{sys}$ according to Equations 15) which describes heat lost across the tank-to-ambient temperature difference ($T_{3[t=t_{col}]}-\tilde{T}_{a[t_{ret}]}$). A corresponding overall forward mode heat transfer

coefficient can be defined ($U_{f,sys}A_{sys}$, according to Equation 16) to describe heat loss across the tank-to-ambient temperature difference during collection periods ($T_{3[t=t_{col}]} - \tilde{T}_{a[t_{col}]}$). Dynamic modelling of heat loss during retention periods ($-\Delta Q_{T[t_{ret}]}$) and heat gained during collection periods ($\Delta Q_{T[t_{col}]}$) can be performed using Equations 17 and 18 which are essentially the inverse forms of Equations 15 and 16.

$$H_{col} = \int_{t=0}^{t=t_{col}} G \qquad \text{Equation 12}$$

$$\eta_{T,col} = \frac{Energy\ in\ store\ at\ t{=}t_{col}}{Energy\ incident\ from\ t{=}t_0\ to\ t{=}t_{col}} = \frac{M{\cdot}c_p\left(T_{3[t=t_{col}]} - T_{3[t=t_0]}\right)}{H_{col}{\cdot}A_1} \qquad \text{Equation 13}$$

$$\eta_{T,ret} = \frac{Retained\ energy\ in\ store\ at\ t{=}t_{col}{+}t_{ret}}{Energy\ in\ store\ at\ t{=}t_{col}} = \frac{M{\cdot}c_p\left(T_{3[t=t_{col}+t_{ret}]} - \tilde{T}_{a[t_{ret}]}\right)}{M{\cdot}c_p\left(T_{3[t=t_{col}]} - T_{a[t=t_{col}]}\right)} \qquad \text{Equation 14}$$

$$U_{r,sys}A_{sys} = \frac{M{\cdot}c_p}{t_{ret}} \ln\left(\frac{1}{\eta_{T,ret}}\right) \qquad \text{Equation 15}$$

$$U_{f,sys}A_{sys} = \frac{M{\cdot}c_p}{t_{col}} \ln\left(\frac{1}{\eta_{T,col}}\right) = F \cdot U_L A_1 \qquad \text{Equation 16}$$

$$-\Delta Q_{T[t_{ret}]} = Q_{T[t=t_{col}]} \frac{T_{3[t=t_{col}]} - \tilde{T}_{a[t_{ret}]}}{T_{3[t=t_{col}]} - T_{a[t=t_{col}]}} \left(1 - \left[e^{\frac{U_{r,sys}\,A_{sys}\,t_{ret}}{M{\cdot}c_p}}\right]^{-1}\right) \qquad \text{Equation 17}$$

$$\Delta Q_{T[t_{col}]} = F \cdot A_1 \left(H_{col} \cdot \tau \cdot \alpha - t_{col}\, U_L\left(T_{3[t=t_0]} - T_{a[t=t_0]}\right)\right)\left[e^{\frac{F{\cdot}U_L\,A_1\,t_{col}}{M{\cdot}c_p}}\right]^{-1} \qquad \text{Equation 18}$$

Heat could feasibly be drawn from the ICSSWH to serve a variety of thermal load demands at different times of the day (eg morning or evening bathing, space heating at night, etc). If all available heat is consumed during a single short duration draw-off event occurring once every 24h, the maximum availability of stored heat ($Q_{T,24max}$, Equation 19) occurs when the tank temperature reaches its maximum (near the end of the collection period, usually just before dusk) and minimum availability of stored heat ($Q_{T,24min}$, Equation 20) coincides with the time when the lowest tank temperature occurs (near the end of the retention period, usually around dawn). Provided that t_{col} and t_{ret} cover a contiguous 24h period then the product of the collection and retention efficiencies can reasonably be described as the diurnal thermal efficiency, where $\eta_{T,24}=1$ if all available solar energy incident during t_{col} is collected and then retained without loss for the duration of t_{ret}, or $\eta_{T,24}=0$ if no heat was collected or all collected heat was lost. The total diurnal efficiency ($\eta_{T+E,24}$) is the sum of the diurnal thermal efficiency and the diurnal electrical efficiency ($\eta_{E,24}$) and can be defined according to

Equation 21. It is important to note that diurnal thermal efficiency (by this definition) is a relative measure of long-term performance and that non-zero values do not necessarily imply net heat gain in a given 24h period. For example, heat gained on a cloudy day following several warm sunny days could well be less than the amount of heat lost during a subsequent cool night, even with relatively high collection, retention and diurnal thermal efficiencies.

$$Q_{T,24max} = \eta_{T,col} \cdot \mathrm{A}_1 \cdot H_{col} \qquad \text{Equation 19}$$

$$Q_{T,24min} = \eta_{T,col} \cdot \eta_{T,ret} \cdot \mathrm{A}_1 \cdot H_{col} \qquad \text{Equation 20}$$

$$\eta_{T+E,24} = \eta_{T,24} + \eta_{E,24} = \eta_{T,col} \cdot \eta_{T,ret} + \frac{1}{t_{col}} \int_{t=0}^{t=t_{col}} \frac{q_E}{G \cdot A_1} \qquad \text{Equation 21}$$

Table 2 summarises performance values reported in previous experimental studies on ICSSWH collector prototypes to serve as benchmarks for the devices examined in this and future studies. A confusing variety of metrics and test methodologies are reported in the literature, but most can be readily interpreted and converted into $\eta_{T,col}$, $\eta_{T,ret}$, and $U_{r,sys}A_{sys}$ parameters according to the definitions given above. It is important to ensure that the solar thermal condition is properly accounted for when comparing reported collection efficiencies because $\eta_{T,col}$ inherently reduces with increasing N. Test duration and tank-to-ambient temperature difference must be borne in mind when comparing retention efficiencies because $\eta_{T,ret}$ inherently reduces with increasing t_{ret} and ΔT_{3a}. Likewise, comparisons between heat loss coefficients must be made with caution because there is a lack of consistency concerning definitions for reference areas (these are variably reported based on the absorber, aperture, or whole envelope area) and because $U_{sys}A_{sys}$ inherently increases in proportion to the physical size of the ICSSWH. To enable fair comparisons in relation to heat retention performance, we propose two new heat loss coefficient metrics, one of which is referenced to stored water volume ($U_{r,sys}A_{sys}/u$) and the other of which is referenced to the effective aperture area ($U_{r,sys}A_{sys}/A_1$). The latter has the advantage of being broadly equivalent to $F \cdot U_L$ values reported for conventional solar water heating collectors whereas the former is very useful when drawing comparisons between ICSSWH collectors with very different storage tank sizes and shapes. It should be noted that the data reported in Table 2 is drawn from a variety indoor and outdoor tests for which the influences of variables such as wind speed (which affects heat losses) and solar incidence angle (which affects optical losses) cannot easily be determined. Data in Table 2 suggests a state-of-the-art benchmark ICSSWH collection efficiency of $\eta_{T,col} \approx 60\%$ at $N \approx 0.035 m^2K \cdot W^{-1}$

(comparable to efficiencies achieved by basic conventional solar thermal collectors, refer to Figure 3) and state-of-the-art benchmark heat loss coefficients of $U_{r,sys}A_{sys}/A_1 \approx 1$ W·m^{-2}K^{-1} and $U_{r,sys}A_{sys}/u \approx 10$ W·m^{-3}·K^{-1} at $\Delta T_{3a} \approx 25$°C (equivalent to a 100L cube shaped tank fully insulated on all sides with 30mm insulation of conductivity k=0.025 W·m^{-1}K^{-1}).

Table 2: Performances of ICSSWH collectors reported in the literature

ICSSWH description	Solar thermal collection efficiency	Over-night heat retention efficiency	Test duration	Overall heat loss coefficient	Effective aperture area	Water storage vessel volume	Aperture specific heat loss coefficient	Volume specific heat loss coefficient
	$\eta_{T,col}$	$\eta_{T,ret}$	$t_{col} + t_{ret}$	$U_{r,sys}A_{sys}$	A_1	u	$\frac{U_{r,sys}A_{sys}}{A_1}$	$\frac{U_{r,sys}A_{sys}}{u}$
	(%)	(%)	(hours)	(W·K^{-1})	(m^2)	(L)	(W·m^{2}K^{-1})	(W·m^{3}K^{-1})
Near-triangular trapezoidal prism tank, single glazed, 25mm insulation. Thermosiphonically coupled absorber channel, thermal diode reverse flow stop valve. (Mohamad, 1997)	53*	66	12+12	4*	0.55	100	7.3*	40*
Semi-flat trapezoidal tank, double (?) glazed, 50mm insulation. Thermosiphonically coupled absorber channel, thermal diode reverse flow stop valve. (Faiman et al., 2001)	34	84	11+8.5	2.8	1.15	120	2.4	23
Horizontal cylindrical tank, two-part CPC reflector, single glazed. (Tripanagnostopoulos et al., 2002)								
STS-1A & 2A: Single tank	41	58	12+12	5.3	0.95	100	5.6	53
STS-1B & 2B: Modified reflector	48	57	12+12	5.5	0.95	100	5.8	55
DTS-2B: Double tanks, modified reflector	50	50	12+12	6.7	0.95	100	7.1	67
Cylindrical tank, selective coating, two-part CPC reflector, single glazed, insulated. (Smyth et al., 2003)								
A2: Basic design	52	45	8+16	4.2	0.92	57	4.6	74
A4: Internal perforated sleeve added	58	53	8+16	3.4	0.92	57	3.7	60
A8: extra insulation added	59	61	8+16	4	0.92	85	4.3	47
Close-coupled tubular absorber on top of a flat cuboid tank with bulbous head. Tank fully enclosed with 40mm insulation. (Sopian et al., 2004)								
1: Free thermosiphonic flow	45	18	8+16	40.9	2.30	329	17.8	124
2: Thermal diode reverse flow stop valve	45	52	8+16	15.6	2.30	329	6.8	47
Double horizontal cylindrical tanks, three-part CPC reflector, single glazed, insulated. Tripanagnostopoulos & Souliotis (2006)								
DTS-B2 reflector design variant	55	53	12+12	6.5	1.01	107	6.4	61
DTS-C2 reflector design variant	46	59	12+12	5.5	0.75	107	7.3	51
Horizontal cylindrical tank-in-tank, selective coating, two-part CPC reflector, single glazed, insulated. Air-filled annulus. (Souliotis et al., 2011)	33	66	12+12	1.5	0.83	44	1.8	34

Cuboid tank, selective coating on underside, 50mm insulation elsewhere. Single glazed aperture with reflectors (1.8x CPC, reverse circular & straight) directing light onto inverted absorber. (Smyth et al., 2005)								
1: No baffles in reflector	43	86	8+16	0.81	0.36	38	2.3	21
2: Two full-width transparent baffles	40	92	8+16	0.45	0.36	38	1.3	12
7: One half-width transparent baffle	46	85	8+16	0.84	0.36	38	2.3	22
Horizontal cylindrical tank, selective coating, two-part CPC reflector, glazed, insulated. (Souliotis et al., 2013)								
3A: Single glazing	54	61	12+12	4.85	1.48	102	3.3	48
3B: Double glazing	53	65	12+12	4.2	1.48	102	2.8	41
Horizontal cylindrical tank-in-tank, selective coating, two-part CPC reflector, single glazed, insulated. Evacuated annulus part-filled with water to form a thermal diode (Souliotis et al., 2017)								
Starting pressure 86mbar	29	74	12+12	1.29	0.83	44	1.6	29
Starting pressure 998mbar	31	68	12+12	1.66	0.83	44	2.0	38
Vertical cylindrical tank-in-tank, matt black, transparent plastic cylindrical cover, insulated ends. Evacuated annulus (38mbar) with pumped thermal diode. (Smyth et al., 2018)	36*	61	6+18	0.9	0.32	28	2.9	32
Horizontal cylindrical tank-in-tank, matt black, transparent plastic cylindrical cover, insulated ends. Evacuated annulus part-filled with water to form a thermal diode (Muhumuza et al., 2019)								
1: Aluminium outer vessel, no capillary	28*	25	6+18	1.5	0.24	17	6.1	88
2: Stainless steel outer vessel + capillary	31*	40	6+18	1	0.24	17	4.1	59
3: As variant 2 but longer vessels	29*	48	6+18	1.3	0.40	28	3.2	46
Horizontal rectangular tank, matt black, insulated on 5 sides with double glazed cover (Harmim (2019)	47	93	12+12	2.6	1.13	60	2.3	43
Benchmarks								
Minimum reported in literature	28						1.3	12
Average reported in literature	43						4.6	49
Maximum reported in literature	59						17.8	124
Targets for ICSSWH development	**60**						**1.0**	**10**

Collection efficiencies reported in the table relate to an average daily solar thermal condition of N=0.035±0.005 $m^2K \cdot W^{-1}$. Retention efficiencies and heat loss coefficients reported in the table relate to a normalised stored water temperature of ΔT_{3a} = 25±10°C (averaged over the retention period). Exceptions where data relates to N ≈ 0.01 $m^2K \cdot W^{-1}$ and ΔT_{3a} ≈ 10°C are marked with asterisk*. Reported values of A_1 relate to the transparent aperture area (excluding external framing elements) which is typically the same as the absorber area for non-concentrating ICSSWH devices.

2.6 Planar Liquid-Vapour Thermal Diodes

A thermal diode is a unidirectional heat transfer device that operates in a manner analogous to an electrical semiconductor diode by offering low resistance (thermal conductance) in one direction and high resistance (thermal insulation) in the other. Thermal diode devices have been used to successfully reduce heat loss via reverse flows in thermosiphonic solar water heaters (one-way valves employed by Mohamad, 1997; Faiman et al., 2001; Sopian et al., 2004), to promote stratification in hot water storage tanks (Smyth et al., 1999 and Rhee et al., 2010), and to reduce overnight heat losses from ICSSWH absorbers (De Beijer, 1998; Quinlan, 2010; Souliotis et al., 2011&2017;

Smyth et al., 2015a&b, 2017, 2018, 2019; Pugsley et al., 2016 & 2017; Muhumuza et al., 2019a&b and 2020).

Planar Liquid-Vapour Thermal Diodes (PLVTD) consist of two parallel plates of area A=yz separated by a cavity of depth x which contains a quantity of working fluid maintained in a thermodynamic state close to saturation (Pugsley et al., 2019 & 2020). During forward mode operation, wetting of the hottest plate (evaporator) through contact with the liquid working fluid generates vapour, which then migrates to the colder plate (condenser) where it releases its latent heat and generates condensate to complete the cycle. During reverse mode operation, the hottest plate is kept dry so that no vapour can be generated, no latent heat transfer occurs, and the partially evacuated cavity acts as an insulator (see Figure 4). Requirements, functions and interactions of the main PLVTD components can be summarised as follows, based on Pugsley et al. (2017 & 2020):

- **Evaporator and condenser plates** should be formed of thermally conductive material and should be as thin as possible to maximise forward mode heat transfer. Choice of plate thickness is also governed by the inherent need to prevent structural deformation caused by implosion forces associated with the combination of cavity vacuum and external atmospheric pressure. Internal supporting structure is generally required in large PLVTDs. Hermetic sealing is required to prevent infiltration of non-condensable gases.
- **Cavity sidewalls and internal structure** should have low thermal conductivity to minimise bridging that would otherwise cause unwanted reverse mode heat transfer. These elements must provide sufficient structural strength to prevent deformation and should be formed of low-outgassing materials to avoid risk of vacuum degradation (also applies to plates and seal materials). Internal structures must not significantly impede vapour flows between the plates in order to avoid impairing forward mode heat transfer.
- **Working fluid** selection considerations include saturation pressure at operating temperature, specific heat capacity, liquid & vapour thermal conductivities, liquid & vapour viscosities, latent heat of vaporisation, cost, flammability, toxicity, global warming and ozone depletion potential. Water appears to be a suitable fluid. Determination of required quantity involves consideration of plate area, cavity volume, the need to minimise thermal inertia, and the need to avoid evaporator dry-out at high temperatures. Working fluid reservoirs should be designed to prevent thermal bridging between the plates.

- **Evaporator wetting and condensate return mechanisms** must ensure continuous and uniform working fluid flows during forward mode operation and should preferably maintain dry plates in reverse mode. Evaporator hydrophilicity and condenser hydrophobicity are important considerations. Evaporator wetting can be achieved by a variety of active (eg pumped falling film or spray) or passive (eg capillary wick or pockets) techniques. Consideration should be given to parasitic energy consumption by pumps in active systems.

Experimental and theoretical work by Pugsley et al. (2016, 2017, 2019 & 2020) demonstrated that large vertical PLVTDs ($A=0.98m^2$ and $x=70mm$ deep) suitable for integration in façade mounted ICSSWH collectors can be realised to achieve reverse mode insulation of $U_r<2$ $W{\cdot}m^{-2}K^{-1}$ and forward mode heat transfer in the range $50<U_f<900$ $W{\cdot}m^{-2}K^{-1}$. Reverse mode insulation is determined by PLVTD dimensions such that thermal conductance decreases with increasing depth. Forward mode heat transfer is highly dependent upon PLVTD operating conditions such that thermal conductance increases with increasing temperature and increasing heat flux but is relatively insensitive to PLVTD dimensions.

Using a vertical PLVTD as the connecting element between PV cells and water storage tank in a BIPV-ICSSWH facade system has the potential to not only reduce ICSSWH heat losses by improving tank insulation, but also to improve thermal and electrical collection efficiencies by improving heat transfer. Given that PLVTDs essentially act as heat spreaders (Boreyko and Chen, 2013) there is also potential for electrical efficiency improvements associated with improved PV cell temperature uniformity.

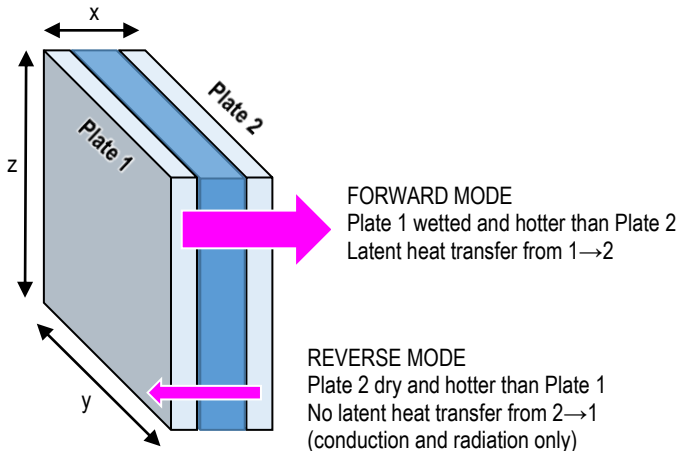

Figure 4: Schematic diagram of a PLVTD

3 Theoretical understanding of a BIPV-PLVTD-ICSSWH

3.1 Energy balance model

The fundamental physical arrangement of the BIPV-PLVTD-ICSSWH device proposed in Figure 1 can be represented by the lumped parameter model shown in Figure 5 and the equivalent resistance network shown in Figure 6. The model describes how the input solar flux (G) is absorbed by the PV cells (at temperature T_0) where it is converted to thermal energy and electrical energy. The thermal power is either lost (q_{0a}) to the ambient environment (at temperature T_a) or transferred through the thermal diode (q_{03}) to heat the water storage tank (at temperature T_3) where it becomes available for delivery to thermal loads (q_T). Heat transferred from the absorber to the stored water passes through the diode (R_{12}) and storage tank mantle (R_{23}) thermal resistances. Some of the solar heat gained by the tank is lost through the insulated tank sidewalls and back plate (q_{3a} through $R_{3i}+R_{ia}$). Heat losses through the insulated thermal diode sidewalls (q_{4a}) are neglected as these are small by comparison. Absorber heat losses (q_{1a}) pass through the absorber laminate (R_{15}), transparent cover (R_6), airgap (R_{56}) and ambient (R_{6a}) thermal resistances which act in series to determine the overall absorber loss resistance (R_{1a}). It is assumed that each element is isothermal and that heat fluxes are constant across the plane of each element. The amount of electrical power produced by the PV cell array ($q_E=I_{PV}.V_P$) is dependent upon the irradiance (G); the pump and load electrical resistances (R_P+R_{load}); and the PV cell array electrical characteristics (represented by R_{PV}) which are themselves dependent upon the cell material properties and temperature. Some of the electrical power generated by the PV is delivered to a small pump (q_p) which distributes a working fluid film to wet the PLVTD evaporator and the remainder (q_E) is available to serve applied electrical loads (R_{load}). It is assumed that all electrical energy used to drive the pump is eventually converted to heat which is added to the stored water ($q_{P,T}=q_{P,E}=I_P.V_P$).

Collection behaviour of the BIPV-PLVTD-ICSSHW can be modelled by considering the energy balances within the absorber laminate (Equation 22), storage tank (Equation 23), and connected electrical load (Equation 24) by accounting for the transparent cover transmissivity (τ); the absorber surface area (A_1) and absorptivity (α); and the electrical currents flowing from the PV output (at voltage V_P) to ground through the PV, pump and load (I_{PV}, I_P and I_{load} respectively). It should be noted that the optical efficiency ($\tau\alpha$) is dependent upon the solar incidence angle. Substituting Equation 24 into Equation 1, and the resultant expression into Equation 23, yields Equation 25 which describes overall thermal power output. In cases where the pump is fed from an external power supply (as occurred for solar simulator laboratory tests described in Part 2 of 2) the overall thermal power output is described by Equation 26.

$$\tau \cdot \alpha \cdot G \cdot A_1 = q_E + q_P + q_{03} + q_{0a} \quad \text{Equation 22}$$

$$q_T = q_{03} + q_P - q_{3a} \quad \text{Equation 23}$$

$$q_E = q_{PV} - q_P = V_P(I_{PV} - I_P) = V_P I_{load} \quad \text{Equation 24}$$

$$q_T = \tau \cdot \alpha \cdot G \cdot A_1 - V_P I_{load} - q_{0a} - q_{3a} \quad \text{Equation 25}$$

$$q_T = \tau \cdot \alpha \cdot G \cdot A_1 - V_P(I_{PV} + I_P) - q_{0a} - q_{3a} \quad \text{Equation 26}$$

Inspection of the thermal resistance network in Figure 6 indicates that absorber heat loss (q_{0a}) can be expressed in terms of normalised absorber temperature ($\Delta T_{0a}=T_0-T_a$) and the series thermal resistances $R_{05}+R_{56}+R_6+R_{6a}$ to create Equation 27. Tank heat loss (q_{3a}) and tank heat gain (q_{03}) can likewise be expressed in terms of normalised tank temperature ($\Delta T_{3a}=T_3-T_a$) and the absorber-to-tank temperature difference ($\Delta T_{03}=T_0-T_3$) together with relevant thermal resistances to create Equations 28 & 29.

$$q_{0a} = \frac{T_0 - T_a}{R_{05}+R_{56}+R_6+R_{6a}} = \frac{\Delta T_{0a}}{R_{0a}} \quad \text{Equation 27}$$

$$q_{3i} = \frac{T_3 - T_a}{R_{3i}+R_{ia}} = \frac{\Delta T_{3a}}{R_{3a}} \quad \text{Equation 28}$$

$$q_{03} = \frac{T_0 - T_3}{R_{01}+R_{12}+R_{23}} = \frac{\Delta T_{03}}{R_{03}} \quad \text{Equation 29}$$

During collection, absorbed solar radiation is converted to heat and electricity in accordance with the absorber laminate energy balance. Substituting Equations 27 & 28 into Equation 25; and substituting Equations 28 & 29 into Equation 23; yields Equations 30 & 31 which describe the maximum amount of thermal power that the tank can deliver over a sustained period. Substituting Equations 27 & 29 into Equation 22 and rearranging into Equation 32 allows the absorber temperature (T_0) to be evaluated. Substituting Equation 30 into Equation 9 allows the solar thermal collection efficiency to be evaluated according to Equation 33. It should be noted that the term $V_P I_P$ is only relevant when pumping power for the PLVTD evaporator wetter is supplied by the PV cells.

$$q_T = \tau \cdot \alpha \cdot G \cdot A_1 - V_P I_{load} - \frac{T_0 - T_a}{R_{0a}} - \frac{T_3 - T_a}{R_{3a}} \quad \text{Equation 30}$$

$$q_T = \frac{T_0 - T_3}{R_{03}} + V_P I_P - \frac{T_3 - T_a}{R_{3a}} \quad \text{Equation 31}$$

$$T_0 = \frac{(R_{03}R_{0a})(\tau \cdot \alpha \cdot G \cdot A_1 - q_E - q_P) + T_a R_{03} + T_3 R_{0a}}{R_{03}+R_{0a}} \quad \text{Equation 32}$$

$$\eta_T = \frac{{}^{(T_0 - T_3)}/_{R_{03}} - {}^{(T_3 - T_a)}/_{R_{3a}} + (V_P I_P)}{G \cdot A_1} \quad \text{Equation 33}$$

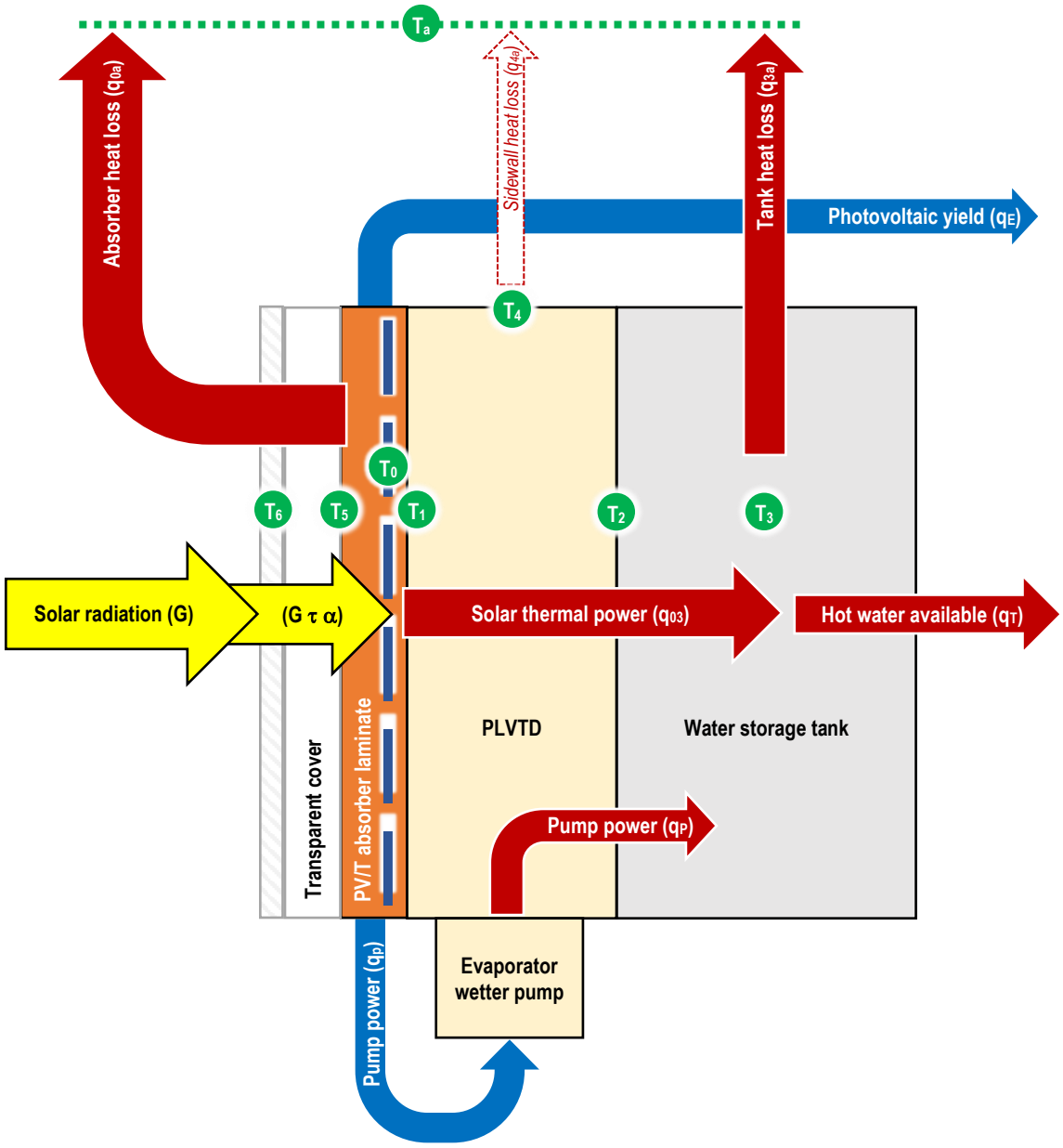

674

675

T_a	Ambient environmental temperature	G	Incident solar radiation flux
T_0	Photovoltaic cell temperature	$G\tau\alpha$	Absorbed solar radiation
T_1	Temp. of absorber laminate substrate and evaporator	q_{03}	Thermal power transferred from the absorber to the water storage tank through the thermal diode
T_2	Temperature of condenser plate and tank mantle	q_T	Net rate of heat gained by the stored water bulk
T_3	Temperature of water bulk stored in the tank	q_{0a}	Absorber heat loss rate
T_4	Thermal diode sidewall temperature	q_{3a}	Rate of heat loss from the back and sides of the water storage tank not covered by the thermal diode
T_5	Absorber laminate surface temperature	q_E	Net electrical power yielded
T_6	Transparent cover temperature	q_P	Electrical power consumed by the evaporator wetter pump which is then all converted to heat

676 ***Figure 5: Lumped parameter model of a BIPV-PLVTD-ICSSWH***

677

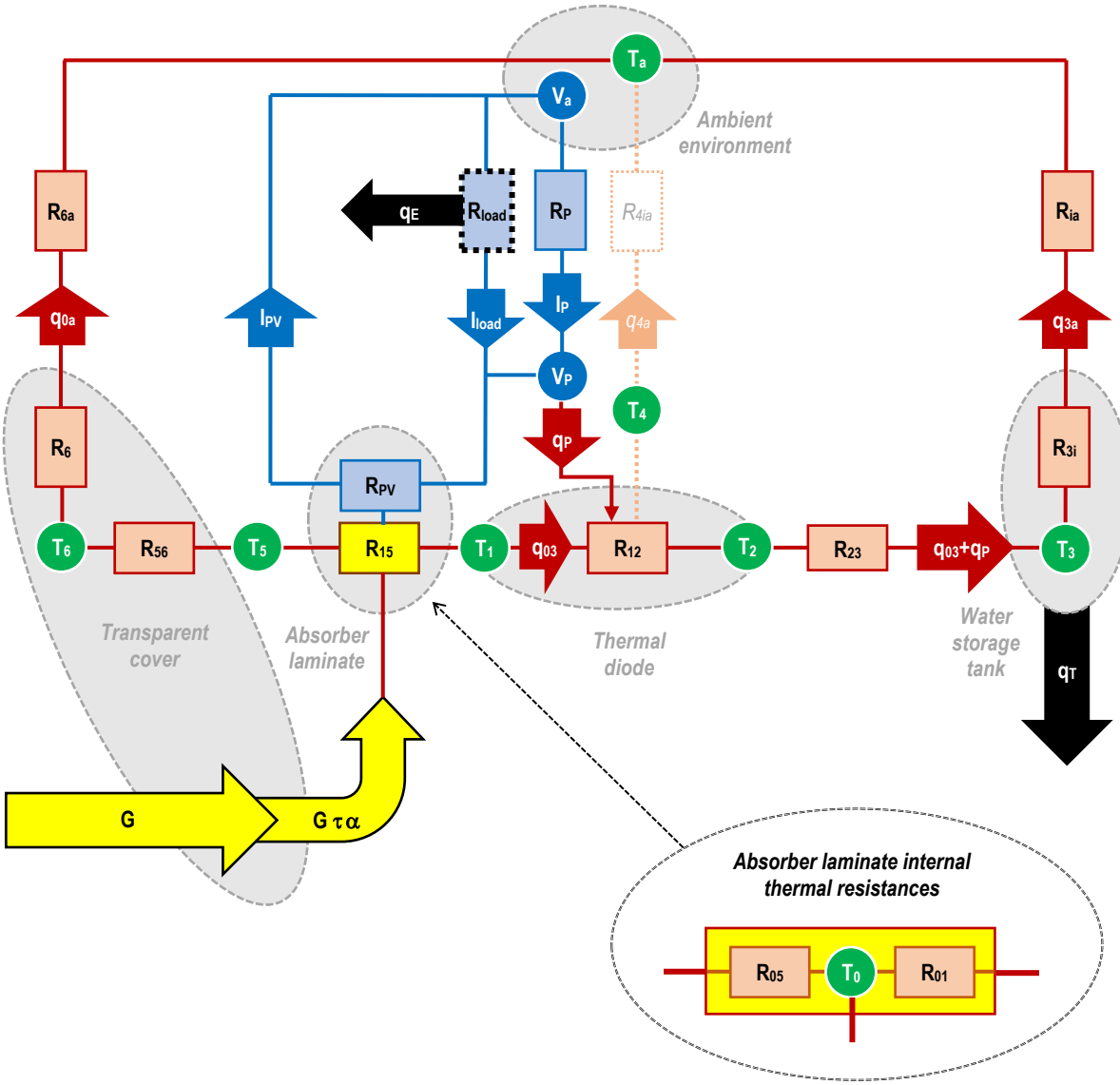

678
679

$G\tau\alpha$	Absorbed solar radiation	V_P	Evaporator wetter pump supply voltage
q_{T+E}	Thermal and electrical power available for use	V_a	Earth electrical potential (zero voltage)
q_{0a}	Heat lost from the absorber	I_{PV}	Current delivered by the photovoltaic module
q_{03}	Solar thermal power transferred to tank	I_{load}	Current drawn by the load
q_{3a}	Heat lost from the water storage tank	I_P	Current drawn by the evaporator wetter pump
q_P	Wetter pump power (electrical becomes thermal)	R_{load}	Electrical load connected to photovoltaic module
R_{1a}	Overall absorber heat loss thermal resistance	R_{PV}	Electrical resistance of photovoltaic module
R_{23}	Water storage tank mantle thermal resistance	R_P	Electrical load of the evaporator wetter pump
$R_{3i}+R_{ia}$	Water storage tank back and side insulation	T_a	Ambient environmental temperature
R_{4ia}	Thermal diode sidewall insulation (assumed infinite)	T_0	Photovoltaic cell temperature
R_{56}	Air gap between absorber and transparent cover	T_1	Absorber substrate & evaporator plate temperature
R_6	Transparent cover thermal resistance	T_2	Temperature of condenser plate and tank mantle
R_{6a}	External air convection & radiation to ambient	T_3	Temperature of water bulk stored in the tank
R_{15}	Absorber laminate thermal resistance	T_4	Thermal diode sidewall temperature
R_{01}	Thermal resistance of laminate behind cells	T_5	Absorber laminate surface temperature
R_{05}	Thermal resistance of laminate in front of cells	T_6	Transparent cover temperature

680 ***Figure 6: Thermal and electrical resistance network for a BIPV-PLVTD-ICSSHW***

$$U_{r,sys} = \frac{1}{A_{sys}}\left[\frac{1}{R_{3a}} + \frac{1}{(R_{03}+R_{0a})}\right] \quad \text{Equation 34}$$

$$\eta_{T,ret} = \frac{M\cdot c_p \Delta T_{3a[t=t_{col}]} - t_{ret}\left[\left(\bar{T}_{3[t_{ret}]} - \bar{T}_{0[t_{ret}]}\right)/R_{03} - \left(\bar{T}_{3[t_{ret}]} - \bar{T}_{a[t_{ret}]}\right)/R_{3ia}\right]}{Mc_p\left(T_{3[t=t_{col}]} - T_{a[t=t_{col}]}\right)} \quad \text{Equation 35}$$

$$F = \frac{\mathrm{R_{0a}}}{\mathrm{R_{03}}+\mathrm{R_{0a}}}\left[\frac{G\cdot A_1 - q_E}{G\cdot A_1}\right] \quad \text{Equation 36}$$

$$F\cdot U_L = \frac{1}{A_1}\left[\frac{1}{R_{3a}} + \frac{1}{(R_{03}+R_{0a})}\right]\left[\frac{G\cdot A_1 - q_E}{G\cdot A_1}\right] \quad \text{Equation 37}$$

At night when there is no solar radiation ($G=q_E=q_P=0$) the network on Figure 6 simplifies somewhat because the electrical elements become inactive and there is no solar flux component. The tank loses heat to the absorber at the same rate as the absorber loses heat to the ambient such that Equation 22 simplifies to $q_{03}+q_{0a}=0$ and the electrical and optical terms of Equations 30-32 become zero. The heat loss coefficient can be expressed in terms of thermal resistances according to Equation 34. Likewise, combining Equations 14 & 31 yields Equation 35 which enables the heat retention efficiency to be evaluated. Heat removal factor can be evaluated using Equation 36 (obtained from inspection of Figure 6) or Equation 37 (obtained by substituting Equation 34 into Equation 10). It is interesting to note that in the case of a thermal-only collector ($q_E=0$), inspection of Equation 36 confirms that $F\rightarrow 1$ when $R_{0a}\rightarrow\infty$ or $R_{03}\rightarrow 0$; $F\rightarrow 0$ when $R_{03}\rightarrow\infty$ or $R_{0a}\rightarrow 0$; and $F=0.5$ when $R_{03}=R_{0a}$.

3.2 Thermal diodicity and its effect on performance

Diodicity coefficient (ς) is a dimensionless measure of thermal rectification and is a useful performance measure for thermal diodes. It is commonly defined according to Equation 38 as a scalar based on the apparent thermal conductivities (k) of the device in forward (f) heat transfer mode and reverse (r) insulation modes. It can alternatively be written in terms of thermal power (q), heat flux (q/A), thermal conductance (U=k/x), or reciprocal thermal resistance (1/R=UA). A reasonable target for diodicity of PLVTDs in ICSSWH applications would be $\varsigma > 99\%$ to replicate absorber transparent cover arrangements in ICSSWH devices where the insulation of high quality double glazing unit is $U\approx 1.2 W\cdot m^{-2}K^{-1}$ (Twidell & Weir, 2006) and heat transfer across the absorber should be $U>200 W\cdot m^{-2}K^{-1}$ (Dupeyrat et al., 2011, Deng et al., 2019).

$$\varsigma = \frac{k_f - k_r}{k_f + k_r} \qquad (0 \geq \varsigma \geq 1) \quad \text{Equation 38}$$

Heat transfer through the diode component in a BIPV-PLVTD-ICSSWH device is represented in the lumped parameter model by thermal resistance ($R_{12}=1/U_{12}A_1$).

Inspection of Figure 6 highlights that this is a key component in the absorber-to-store thermal resistance $R_{03}=R_{01}+R_{12}+R_{23}$ which has a major influence upon the absorber temperature (T_0), heat removal factor (F) and heat loss coefficients (U_L and U_{sys}) as described by Equations 29-37. Given that the solar thermal and photovoltaic collection efficiencies are dependent upon $F \cdot U_L$ and T_0 respectively, and that the heat retention behaviour is determined by $U_{r,sys}$, it is very clear that the U_{12} of the PLVTD has a major influence upon performance. To quantify this, the model described in the preceding sections has been used to examine how thermal diode resistances affect the performance of a notional BIPV-PLVTD-ICSSWH with $A_1=1m^2$ collection area, u=100L storage tank, and the component properties set out in Table 3.

Pugsley et al. (2019 & 2020) proposed and validated calculation methods and a parametric design approach for evaluating the thermal resistances exhibited by a PLVTD and developed a working prototype. Tests demonstrated that the prototype ($A=0.98m^2$ and x=70mm deep) achieved reverse mode insulation of $U_{r,12}=1.7\ W \cdot m^{-2}K^{-1}$ (equivalent to $R_{12}=0.6$ K/W) and typical forward mode heat transfer of $U_{f,12}=38\ W \cdot m^{-2}K^{-1}$ (equivalent to $R_{12}=0.03$ K/W) corresponding to diodicity of $\varsigma \approx 90\%$. Analysis concluded that an order of magnitude increase in forward mode performance could feasibly be realised by improving evaporator wetting uniformity.

Equations 5-10, 32 & 37 have been used to calculate the results on Figures 7 & 8 which illustrate how varying forward mode thermal conductance ($1<U_{f,12}<1000\ W \cdot m^{-2}K^{-1}$, equivalent to $0.001< R_{12}<1$ K/W) affects the solar thermal collection efficiency ($\eta_{T,col}$) and PV/T performance ratio (PR_{T3}). Low diode thermal conductance impairs absorber-to-tank heat transfer causing high absorber temperatures which increase heat losses (thus poor solar thermal collection efficiencies on Figure 7) and resistive electrical losses (thus poor PV/T performance ratios on Figure 8). The degree to which low diode thermal conductance adversely affects performance is dependent upon operating conditions (G, T_a, T_3, wind speed and electrical loads) but follows a similar trend for all scenarios investigated. A notional "knee" point is apparent at $U_{f,12} \approx 100\ W \cdot m^{-2}K^{-1}$, above which minimal performance benefit is gained for order of magnitude increases. This knee corresponds closely to the point at which the zero-loss solar thermal collection efficiencies of bare and covered collectors are approximately equal ($\eta_{T,col} \approx 75\%$ at $N \approx 0\ m^2K \cdot W^{-1}$, no wind, no load).

The target benchmark solar thermal collection efficiency ($\eta_{T,col} \approx 60\%$ at $N \approx 0.035 m^2K \cdot W^{-1}$ and 2m/s wind speed, established in Table 2) is narrowly missed ($\eta_{T,col} \approx 58\%$) for a covered BIPV-PLVTD-ICSSWH with $U_{f,12} \approx 100\ W \cdot m^{-2}K^{-1}$ but is

achievable under "no wind" conditions or if the diode thermal conductance is increased to $U_{f,12}\approx500$ W·m^{-2}K^{-1}. Whilst Figure 7 clearly shows that a transparent cover and air gap is essential for achieving the solar thermal performance benchmark (this is unachievable for a bare absorber, irrespective of $U_{f,12}$ or wind speed), the PR curves on Figure 8 illustrate how the corresponding reduction in transmissivity reduces the photovoltaic performance. PV/T performance ratios are worst when diode thermal conductance is low, ambient temperature is high, and the collector is operating close to the zero-loss solar thermal condition (N=0). The maximum achievable PR value is limited by the PV cell packing factor which in the modelled case is $A_0/A_1=75\%$ but with careful design could feasibly be $A_0/A_1\approx90\%$ to enable the benchmarks discussed in Section 2.2 to be achieved.

Equations 15, 34 & 37 have been used to calculate the results shown in Figure 9 which illustrate how varying the reverse mode thermal conductance ($0.1<U_{r,12}<100$ W·m^{-2}K^{-1}, equivalent to $0.01< R_{12}<10$ K/W) affects the overall heat loss coefficient ($U_{r,sys}A_{sys}/u$) and the corresponding overnight heat retention efficiency ($\eta_{T,ret}$ for a $t_{ret}=12$h period). It is clear that overnight heat loss increases with increasing diode thermal conductance. High $U_{r,12}$ values worsen vulnerability to wind induced heat losses, especially when the bare absorber is exposed (no cover). On the basis of the $U_{r,12}=1.7$ W·m^{-2}K^{-1} reported by Pugsley et al. (2020), the results suggest that the BIPV-PLVTD-ICSSWH design described by Figure 1 and Table 3 would achieve $\eta_{T,ret}>80\%$ and a heat loss coefficient of $U_{r,sys}A_{sys}/u\approx20$ W·m^{-3}K^{-1} which is better than most of the ICSSWHs encountered in the literature (see Table 2) but somewhat shy of $U_{r,sys}A_{sys}/u<10$ W·m^{-3}K^{-1} benchmark target. Achieving the benchmark would require the reverse mode PLVTD thermal conductance to be $U_{r,12}<0.5$ W·m^{-2}K^{-1}. Further interrogation of the model suggests that diode performance is relatively less important if absorber heat loss is better controlled (double glazing and/or low emissivity surface treatments) or if the tank is poorly insulated.

774 ***Table 3: Basis and assumptions for the modelled BIPV-PLVTD-ICSSWH***

Quantity	Value	Unit	Basis
Volume of water in storage tank (u)	0.1	m^3	Typical tank size reported in literature
Aperture and absorber area (A_1)	1	m^2	Typical absorber size reported in literature
PV cell coverage of absorber area (A_0)	0.75	m^2	15 strings, each formed of 8 quarter-cell pieces (78x78mm)
Depth of PLVTD (x_{12})	70	mm	Dimension as discussed by Pugsley et al. (2020)
Depth of tank (x_3)	100	mm	Tank volume divided by absorber area
Absorber-to-ambient conductance (U_{5a}, bare) 5mm clear acrylic bonded to PV cells, no air gap	10.9*	$W{\cdot}m^{-2}K^{-1}$	Calculated from radiative & convective components as per Twidell & Weir (2006) assumes T_5=50°C, T_a=15°C, ε_5=0.8, ε_6=0.9
Absorber-to-ambient conductance (U_{5a}, covered) as above + 30mm air + 3mm clear acrylic cover	4.0*	$W{\cdot}m^{-2}K^{-1}$	Calculated from radiative & convective components as per Twidell & Weir (2006) assumes T_5=50°C, T_a=15°C, ε_5=0.8
PV cell-to-absorber thermal conductance (U_{01})	400	$W{\cdot}m^{-2}K^{-1}$	Polymer bonding layer 0.5mm, thermal conductivity k=0.2 $W{\cdot}m^{-1}K^{-1}$
PV cell-to-air thermal conductance (U_{05})	40	$W{\cdot}m^{-2}K^{-1}$	Bonded transparent cover 5mm, thermal conductivity k=0.2 $W{\cdot}m^{-1}K^{-1}$
Tank wall-to-water thermal conductance (U_{23})	250	$W{\cdot}m^{-2}K^{-1}$	Natural convection heating of fluid adjacent to a vertical plate for T_2=50°C, T_3=49°C equations recommended by Pugsley et al. (2020)
Tank insulation thermal conductance (U_{3a})	0.25	$W{\cdot}m^{-2}K^{-1}$	Rigid foam insulation 100mm, thermal conductivity k=0.025 $W{\cdot}m^{-1}K^{-1}$
Optical transmissivity (τ, bare) 5mm clear acrylic bonded to PV cells, no air gap	96	%	Estimated from optical reflection and absorption loss analysis offered by Kalogirou (2009) assuming normal incidence.
Optical transmissivity (τ, covered) as above + 30mm air + 3mm clear acrylic cover	88	%	Estimated from optical reflection and absorption loss analysis offered by Kalogirou (2009) assuming normal incidence.
Optical absorptivity of PV cells (α)	90	%	Value suggested by Dupeyrat et al. (2011) for mc-si PV cells
Optical emissivity of encapsulated PV cells (ε)	80	%	Nominal value for PV with bonded polymer cover, from Zondag (2008)
Standard power output of PV cell (q_{STC})	4.24	W	156x156mm pseudo square mc-si M-2BB solar PV cell (Bosch, 2010)
Voltage-temperature coefficient ($K_{V:T}$)	-0.37	%/K	156x156mm pseudo square mc-si M-2BB solar PV cell (Bosch, 2010)
Current-temperature coefficient ($K_{I:T}$)	+0.03	%/K	156x156mm pseudo square mc-si M-2BB solar PV cell (Bosch, 2010)

775 Values were chosen to be representative of the BIPV-PLVTD-ICSSWH prototype used for the experimental work (see Part 2 of 2). Stated values
776 of U_{5a} marked with asterisk* relate to the "no wind" condition. Model accounts for effect of U_{5a} increasing with increasing local wind speed according
777 to the relation offered by Twidell & Weir (2006). Calculations assume that evaporator wetter pump power is negligible ($q_p \approx 0$) and that the external
778 electrical load has a resistance which enables operation at maximum power point.

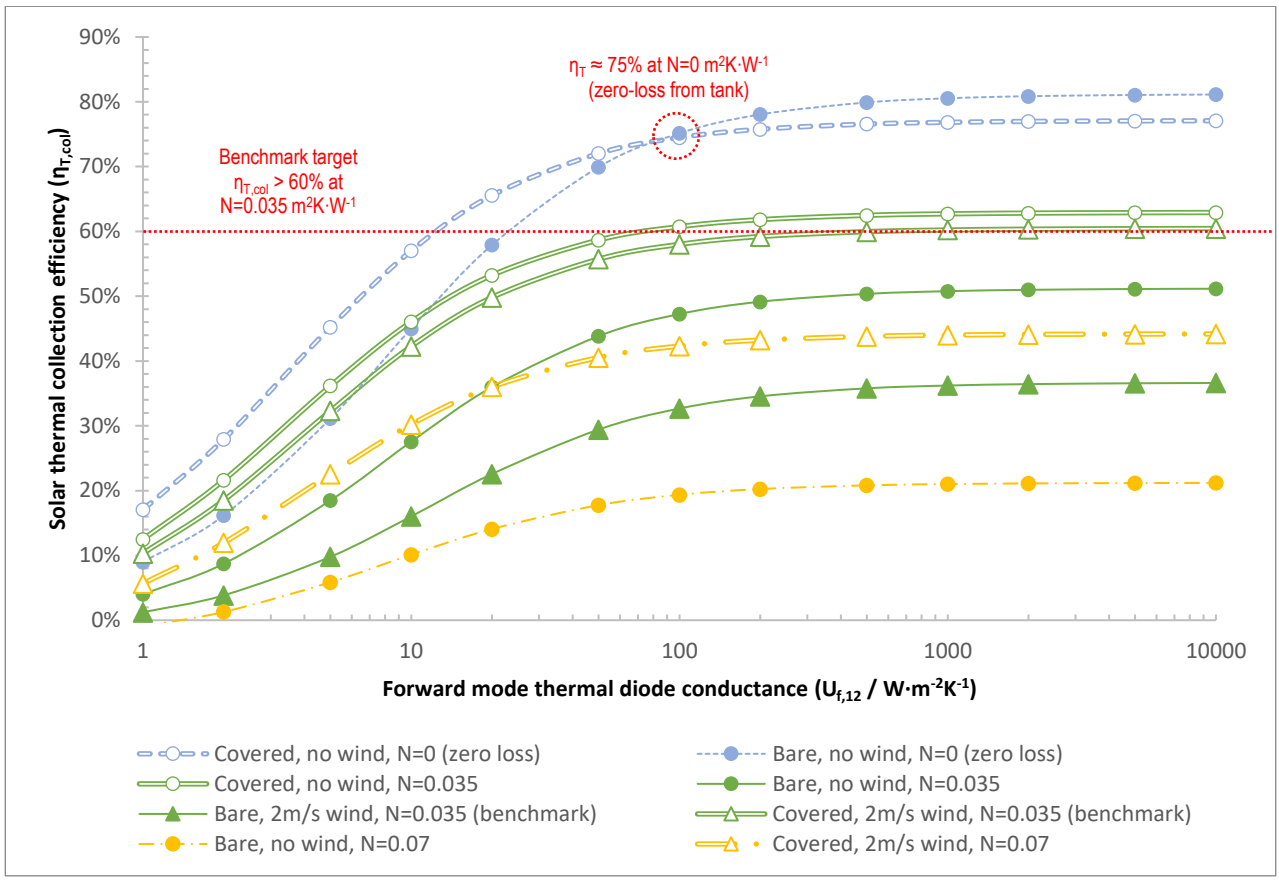

779
780 ***Figure 7: Dependence of solar thermal collection efficiency upon forward mode thermal diode conductance (zero electrical load q_E=0)***

781

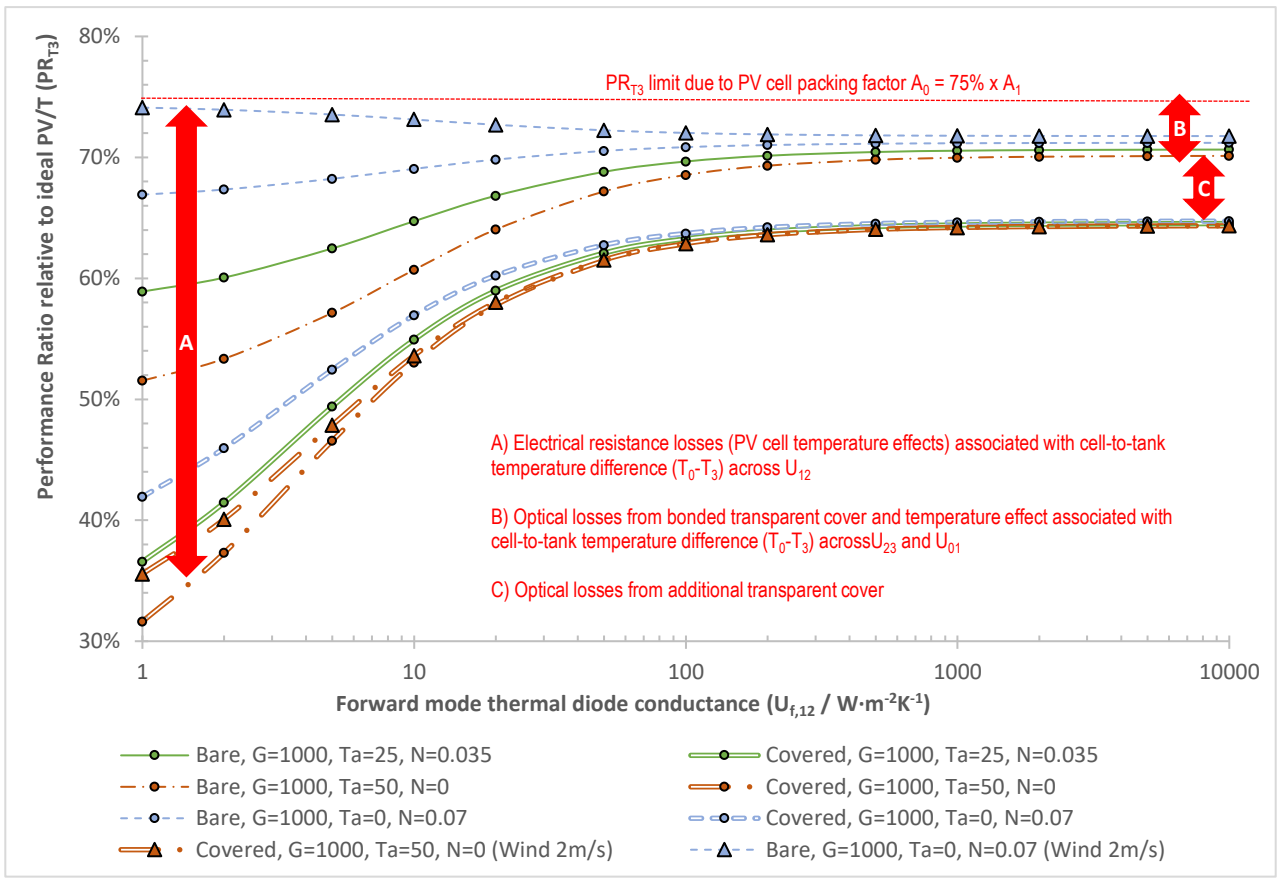

782
783 ***Figure 8: Dependence of PV/T Performance Ratio upon forward mode thermal diode conductance***

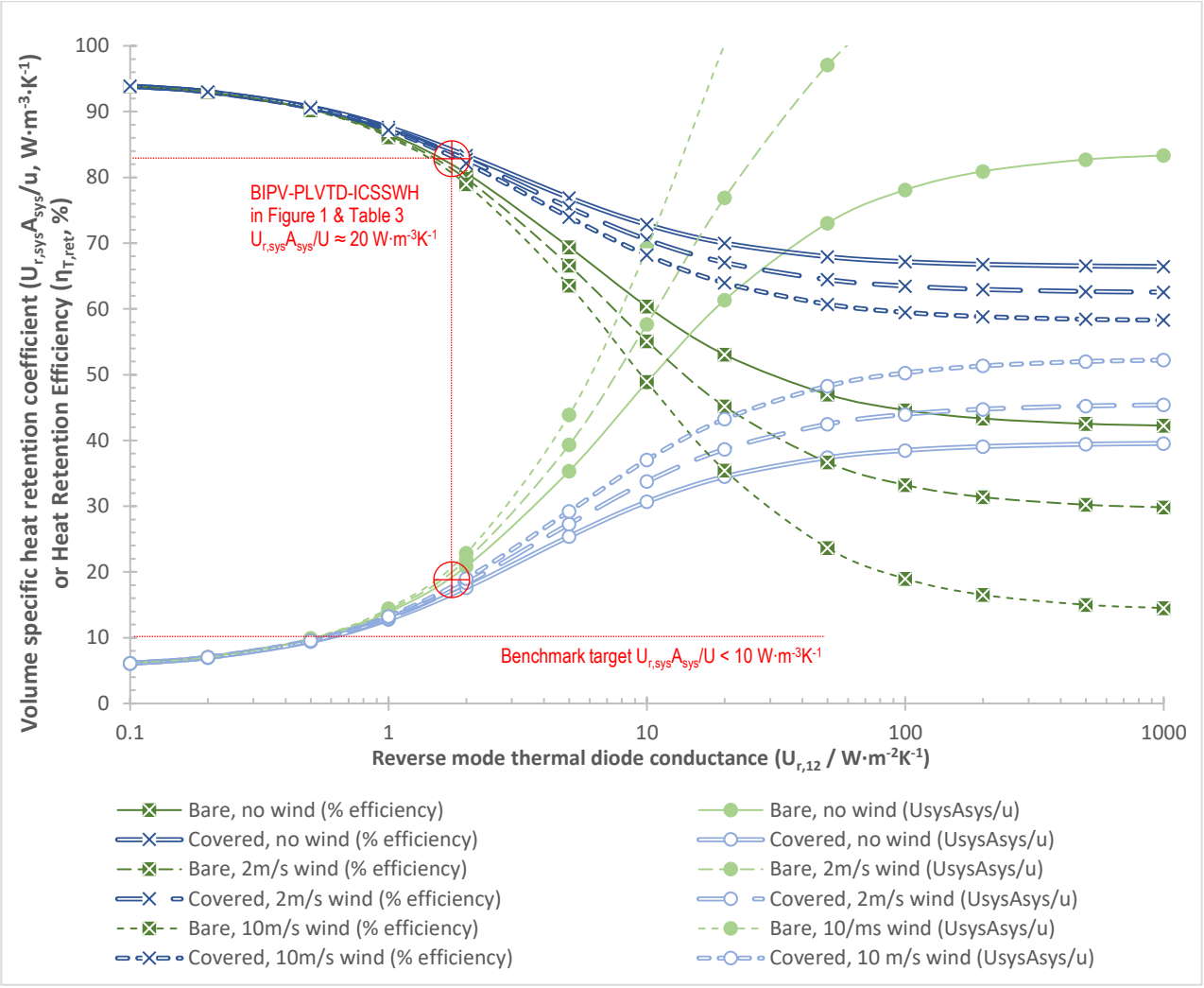

Figure 9: Dependence of overnight heat retention performance upon reverse mode thermal diode conductance

3.3 Behaviour in different climates

Figure 11 compares predicted behaviours of different BIPV-PLVTD-ICSSWH devices to illustrate the overall influence of the PLVTD upon water storage tank temperature (T_3, assumed fully mixed), diurnal thermal efficiency ($\eta_{T,24}$) and maximum power point photovoltaic efficiency ($\eta_{E,mpp}$) over a multi-day period without thermal load (ie no hot water draw-offs). Results were calculated using Equations 5-10, 15-21, 32, 34 & 37 based upon the physical attributes described in Figure 1 and Table 3; a wind speed of 2 m/s; data for summertime average daily solar insolation on a vertical equator facing surface in Rome (H_{24}=12MJ/m^2, see Table 1); and corresponding average ambient temperatures of T_a=25°C during daytime and T_a=19°C at night (NASA, 2019). The three modelled variants are summarised on Figure 10.

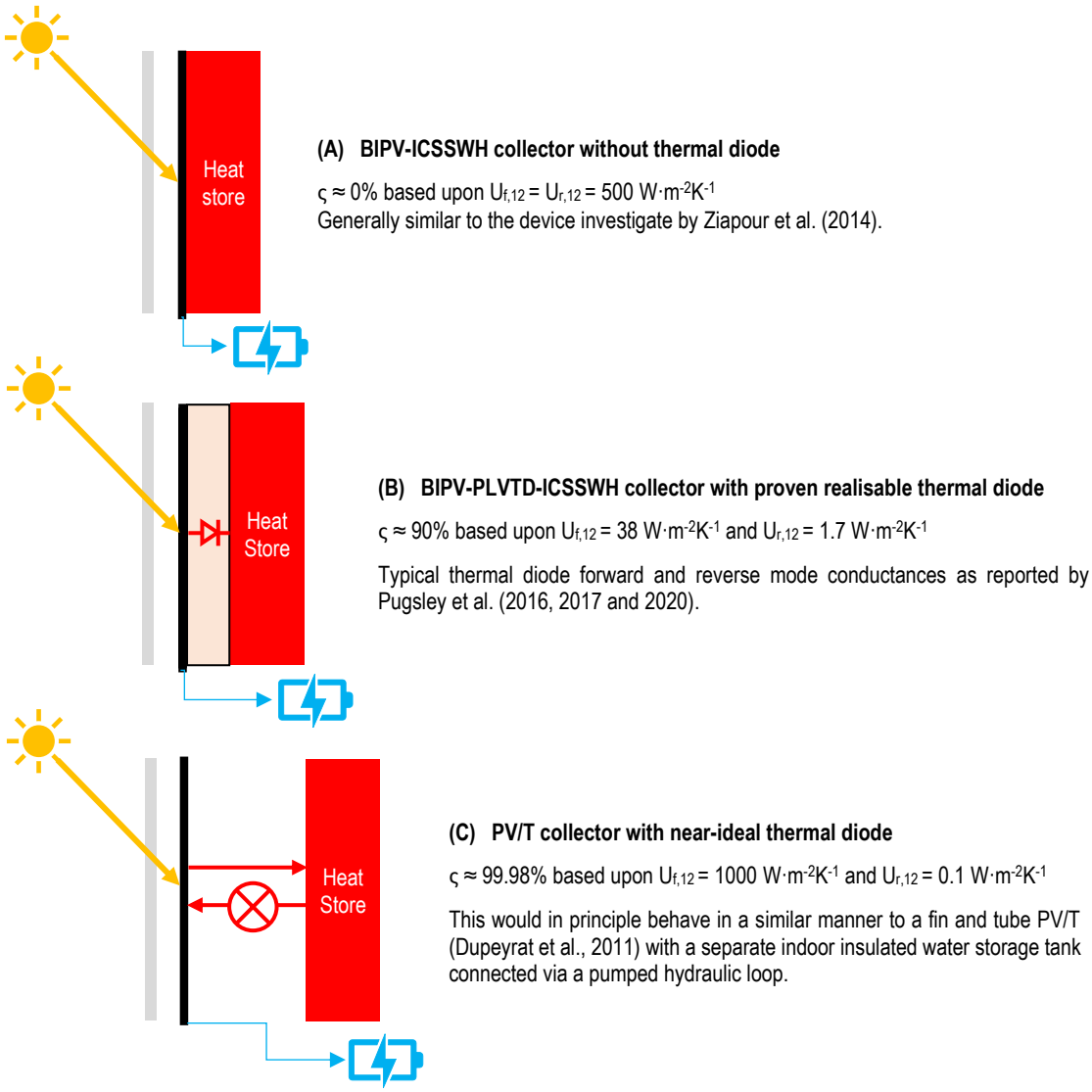

Figure 11: Investigated model variants

Figure 11 shows how tank temperatures (starting at T_3=T_a=25°C) rise each day (solar collection) and fall each night (net heat losses) during an 8-day period of summertime stagnation (eg no thermal load due to a building being unoccupied during vacations). All three device variants achieve similar zero-loss solar thermal efficiencies (η_T≈75% at N=0 m^{2}K·W^{-1} as per Figure 7) and therefore also achieve similar maximum tank temperatures (T_3≈T_a+13≈38°C) and average electrical efficiencies (η_E≈11%) during Day 1. However, their differing overnight heat loss coefficients result in differing tank temperatures by dawn the next day, which causes differences in overall Day 1 diurnal thermal efficiencies ($\eta_{T,24}$=$\eta_{T,col}$·$\eta_{T,ret}$) such that the conventional PV/T with separate tank performs best (Variant C: $\eta_{T,24}$=42%), the BIPV-ICSSWH without thermal diode performs worst (Variant A: $\eta_{T,24}$=28%) and the BIPV-PLVTD-ICSSWH achieves a good compromise (Variant B: $\eta_{T,24}$=35%). After 8 days stagnation, tank temperatures have

risen to T_3=46°C, 55°C and 64°C for Variants A, B and C respectively. Consequently, in terms of Day 8 performances, the conventional PV/T with separate tank performs worst (Variant C: $\eta_{T,24}$=10.6% and η_E≈10.0%) and the BIPV-ICSSWH without thermal diode performs best (Variant A: $\eta_{T,24}$=21.4% and η_E≈10.8%). The device with the BIPV-PLVTD-ICSSWH again achieves a compromise (Variant B: $\eta_{T,24}$=17.1% and η_E≈10.3%). Figure 11 results were calculated based on average summer conditions for a south facing wall in Rome. In practice, the ambient temperatures and insolation levels during a particularly hot and sunny period could be considerably higher than average, and those typically occurring during winter would be notably lower.

Dupeyrat et al. (2011) suggest that 85°C is an appropriate maximum temperature limit for PV/T absorbers constructed using conventional Ethylene Vinyl Acetate (EVA) lamination techniques. Calculations based on H_{24}=20MJ/m^2, T_a=35°C during daytime, and T_a=25°C at night, and no wind, suggest that maximum summertime tank and absorber stagnation temperatures could reach a potentially damaging T_3≈T_0≈106°C in the case of a conventional PV/T (Variant C) but would be maintained at a lower and safer maximum temperature of T_3≈T_0≈86°C in the case of the BIPV-PLVTD-ICSSWH (Variant B) and would reach only T_3≈T_0≈67°C in the case of a simple BIPV-ICSSWH without PLVTD (Variant A). This clearly demonstrates the benefit of the BIPV-ICSSWH concept in respect of minimising stagnation temperatures. In practice, conventional PV/T systems require continuous pumping of heat transfer fluid from the collector to the tank during sunny periods, otherwise much higher absorber stagnation temperatures will occur (T_0>150°C). Inherent electricity demands to run pumps would significantly reduce net electrical yields. By contrast, a BIPV-ICSSWH or BIPV-PLVTD-ICSSWH approach does not require pumps to operate when there is no thermal demand, hence the net electrical yield would be higher than for conventional PV/T.

Calculations for a typical winter scenario in Rome based on H_{24}=12.4MJ/m^2 (see Table 1), T_a=14°C during daytime, and T_a=8°C at night, and 5m/s wind, suggest that the Day 1 diurnal thermal efficiency of a BIPV-PLVTD-ICSSWH (Variant B: $\eta_{T,24}$=30%) would be notably better than that of a BIPV-ICSSWH without PLVTD (Variant A: $\eta_{T,24}$=21%), although slightly worse than for conventional PV/T (Variant C: $\eta_{T,24}$=38%). This clearly demonstrates the benefit of incorporating a PLVTD to reduce overnight heat losses and thus make heat available during the night and early morning hours.

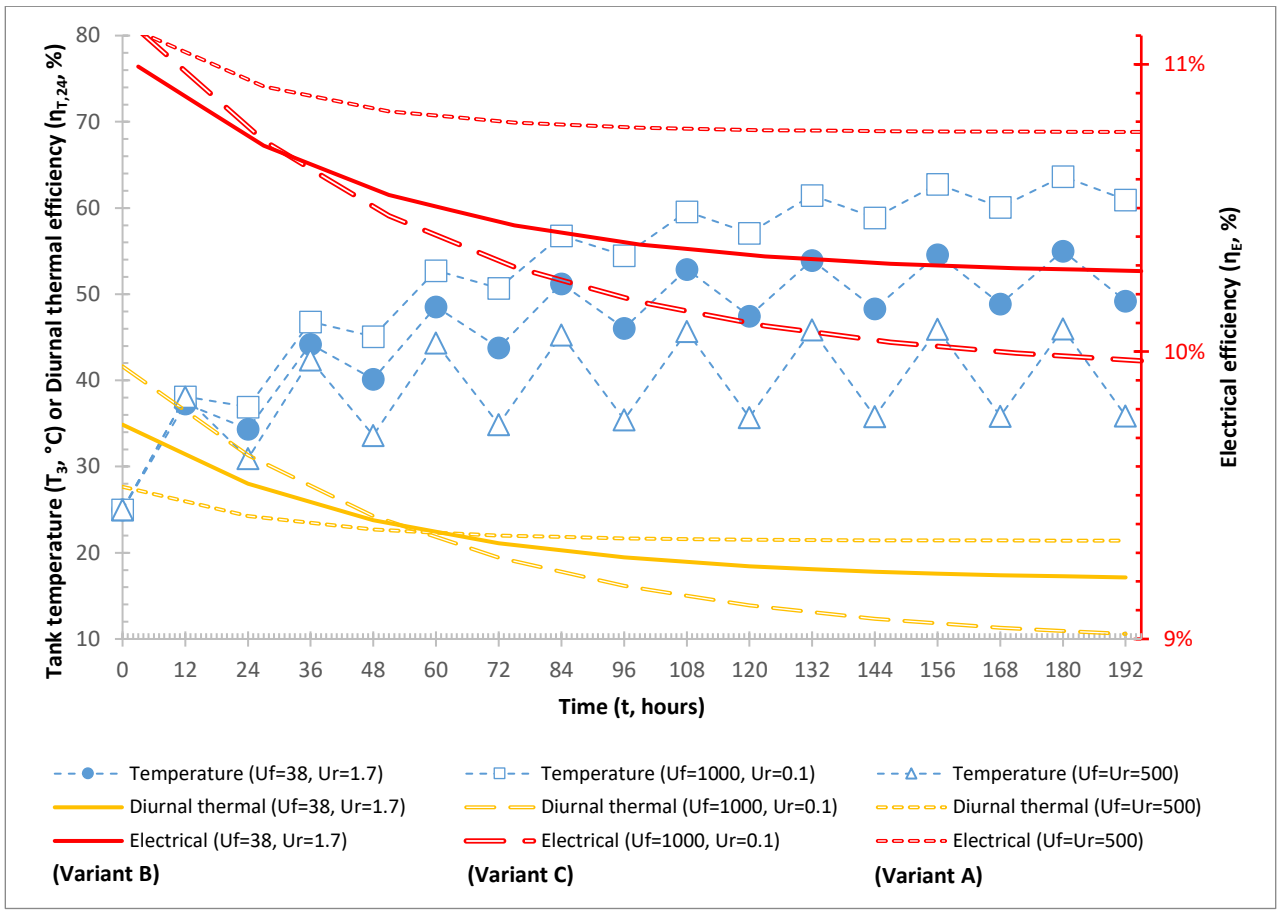

Figure 11: Comparison of tank temperature, diurnal thermal efficiency, and electrical efficiency over a multi-day period

4 Conclusions

This two-part study examines an alternative space-and-energy-efficient approach to BIPV/T which combines BIPV, ICSSWH, and PLVTD concepts. This paper (Part 1 of 2) has reviewed the state-of-the-art for each of the technologies and established the following benchmark performance targets:

- Solar thermal efficiency $\eta_{T,col}$≈60% at N≈0.035m^{2}K·W^{-1} and 2m/s wind speed.
- Heat loss coefficients of $U_{r,sys}A_{sys}/A_1$≈1 W·m^{-2}K^{-1} and $U_{r,sys}A_{sys}/u$≈10 W·m^{-3}·K^{-1} at ΔT_{3a}≈25°C and 2m/s wind speed.
- PV/T performance ratios (relative to an ideal PV/T collector) of PR_{T3}=85% and PR_{T3}=75% for uncovered and covered collectors respectively.

A heat transfer model of a BIPV-PLVTD-ICSSWH façade element was developed to enable solar thermal collection, photovoltaic generation, and overnight heat retention behaviours to be evaluated under various operating scenarios. Subsequent work (presented in Part 2 of 2 of this study) provides experimental validation of the model. The model was interrogated based on notional A_1=1m^2 solar absorber area, 75% PV

cell coverage, and u=100L storage tank to examine how electrical and thermal performances are influenced by PLVTD diodicity characteristics. Key findings can be summarized as follows:

- Increasing forward mode PLVTD thermal conductance improves solar thermal and photovoltaic performances. The degree of improvement gained is dependent upon operating conditions such as irradiance, ambient temperature, heat delivery temperature, wind speed and electrical load.
- Benchmark PV and solar thermal collection targets are achievable if the PLVTD achieves $U_{f,12}$>500 $W \cdot m^{-2}K^{-1}$ and PV cell coverage is >90%, although there is only minimal benefit (<2%) to be gained by increasing forward mode diode thermal conductance above the knee value of $U_{f,12}$≈100 $W \cdot m^{-2}K^{-1}$. Lower PLVTD conductances impair absorber-to-tank heat transfer causing high absorber temperatures which increase heat and electrical losses.
- Reducing reverse mode PLVTD thermal conductance improves overnight heat retention performance. Achieving the target benchmark would require $U_{r,12}$<0.5 $W \cdot m^{-2}K^{-1}$. Excessive heat losses and vulnerability to wind worsen significantly above a notional threshold of $U_{r,12}$≈2 $W \cdot m^{-2}K^{-1}$, especially when the absorber is exposed (no cover).

The model was used to predict the multi-day period behaviour of various BIPV-PLVTD-ICSSWH design and operating scenario variants, without thermal load. Key findings can be summarized as follows:

- During summertime in Rome (insolation H_{24}=12MJ/m^2, wind speed 2 m/s, ambient temperatures T_a=25°C daytime and T_a=19°C at night) diurnal thermal efficiency of $\eta_{T,24}$=35% and average photovoltaic efficiency of η_E≈11% are predicted for the base case PLVTD ($U_{f,12}$=38 $W \cdot m^{-2}K^{-1}$ and $U_{r,12}$=1.7 $W \cdot m^{-2}K^{-1}$). Solar thermal and photovoltaic performances are minimally sensitive to changes in forward mode PLVTD conductance in the range 38<$U_{f,12}$<1000 $W \cdot m^{-2}K^{-1}$.
- Under particularly hot and sunny conditions (insolation H_{24}=20MJ/m^2, no wind, ambient temperatures T_a=35°C daytime and T_a=25°C at night) the model predicts that the base case BIPV-PLVTD-ICSSWH would limit maximum tank and absorber stagnation temperatures to T_3≈T_0≈86°C without the need to operate fluid circulation pumps whereas a conventional PV/T system could reach a potentially damaging T_3≈T_0≈106°C and would require pumps to be energised

continuously during collection periods to prevent even higher (T_0>150°C) temperatures developing.

- Overnight heat retention is very sensitive to changes in reverse mode PLVTD conductance such that increasing or decreasing in the range 0.1<$U_{r,12}$<500 W·m^{-2}K^{-1} changes diurnal thermal efficiency by ±7% relative to the base case ($U_{r,12}$=1.7 W·m^{-2}K^{-1}). Pronounced heat losses occur during winter in the $U_{r,12}$ 500 W·m^{-2}K^{-1} case owing to low ambient temperatures and increased wind speeds and become very reliant on the insulation provided by the transparent cover.

The passive BIPV-PLVTD-ICSSWH approach to controlling overheating significantly reduces the risk of stagnation damage and increases net electrical yields compared to conventional BIPV/T approaches. This alternative approach to BIPV/T could have positive impacts in the context of realising NZEBs as part of global efforts to tackle the climate crisis.

Acknowledgements

This research was enabled in its early stages by studentship funding support from the Northern Ireland Department for the Economy. The work was subsequently progressed with funding support from SolaForm Ltd and was completed as part of the "SolaNetwork" project funded by the UKRI Engineering and Physical Sciences Research Council (EP/T004819/1). The authors would also like to thank networking support funded by the European Union FP7 COST Action TU1205 "Building Integration of Solar Thermal Systems".

Nomenclature

Latin symbols

A	Surface area [m^2]
c_p	Specific heat capacity at constant pressure [J·kg^{-1} K^{-1}]
FF	Photovoltaic Fill Factor [%]
G	Solar irradiance [W·m^{-2}]
H	Solar insolation [MJ·m^{-2}]
I	Electrical current [A]
k	Thermal conductivity [W·m^{-1} K^{-1}]
K	Photovoltaic performance correction coefficients [% or %/K]
m	Mass [kg]
M	Mass flow rate [kg·s^{-1}]
N	Solar Thermal Condition [m^2·K·W^{-1}]
q	Thermal or electrical power [W]
$Q_{[t]}$	Thermal energy, cumulative during time period [MJ]

PR	Performance ratio [%]
R	Thermal or electrical resistance [K·W^{-1}]
t	Time [s]
T	Temperature [°C]
$\tilde{T}_{[t]}$	Average temperature, during time period [°C]
u	Volume [m^3]
U	Thermal conductance or heat transfer coefficient [W·m^{-2} K^{-1}]
V	Electrical voltage [V]
x	Distance along an axis which is parallel to the PLVTD depth [m]
y	Distance along horizontal axis perpendicular to PLVTD depth [m]
z	Distance along an axis which is perpendicular to x and y axes [m]

Greek and other symbols

α	Absorptivity
ε	Emissivity
ΔT	Temperature difference [°C]
η	Efficiency [%]
ς	Diodicity [%]
τ	Transmissivity

Subscripts

0	Photovoltaic cells
1	Planar Liquid-Vapour Thermal Diode, Plate 1 which is the evaporator in forward mode
2	Planar Liquid-Vapour Thermal Diode, Plate 2 which is the condenser on forward mode
3	Hot water storage tank
4	Sidewalls of the Planar Liquid-Vapour Thermal Diode
5	External surface of the solar absorber
6	Transparent element covering solar absorber
0a	Between PV cells and ambient environment
03	Between PV cells and hot water storage tank
1a	Between solar absorber and ambient environment
12	Between (or average of) the two plates
15	Between the PLVTD and the external surface of the solar absorber (through the laminate)
23	Between the PLVTD and the water storage tank
24	Diurnal period of 24 hours
3a	Between water storage tank and ambient environment
3ia	Between water storage tank and ambient environment through insulation
365	Annual period of 365 days
4a	Between PLVTD sidewalls and ambient environment
56	Across the air gap between the solar absorber and transparent cover
6a	Between the transparent cover and the ambient environment
a	Ambient environment
avg	Average
col	Collection (period of solar absorber illumination, eg daytime)
E	Electrical
f	Forward mode
h	Horizontal orientation

inst	Instantaneous
L	Loss to ambient environment
load	Applied electrical load
mpp	Maximum Power Point
oc	Open circuit
P	Pump
PV	Photovoltaic
r	Reverse mode
ret	Retention (period without solar absorber illumination, eg night-time)
sc	Short circuit
STC	At Standard Test Conditions
sys	Whole system
T	Thermal
T3	At the hot water storage tank temperature
I:T	Current-Temperature relationship
V:T	Voltage-Temperature relationship
V:G	Voltage-Irradiance relationship

Abbreviations

a-si	Amorphous silicon
BIPV	Building Integrated PhotoVoltaics
BISTS	Building Integrated Solar Thermal Systems
CdTe	Cadmium Telluride
CIGS	Copper Indium Gallium Selenium
ICSSWH	Integrated Collector-Storage Solar Water Heater
mc-si	Mono-crystalline silicon
NZEB	Net Zero Energy Building
pc-si	Poly-crystalline silicon
PLVTD	Planar Liquid-Vapour Thermal Diode
PV/T	Photovoltaic-Thermal

References

Abdelrazik, A., Al-Sulaiman, F., Saidur, R., Ben-Mansour, R. (2018). A review on recent development for the design and packaging of hybrid photovoltaic/thermal (PV/T) solar systems. Renewable and Sustainable Energy Reviews 95 (2018) 110–129

Amerongen, G., Lee, J., Suter, J. (2013). Legionella and solar water heaters. Report commissioned by the Solar Certification Fund. Available at: <www.estif.org/solarkeymarknew/images/downloads/SCF/scfdeliverables/Report%20SCF%20Legionella%20and%20solar%20water%20heaters%20%20Final%202013%2004.pdf>

Barone, G., Buonomano, A., Forzano, C., Palombo, A., Panagopoulos, O. (2019). Photovoltaic thermal collectors: Experimental analysis and simulation model of an innovative low-cost water-based prototype. Energy 179 (2019) 502-516

Beausoleil-Morrison, I., Kemery, B., Wills, A., Meister, C. (2019). Design and simulated performance of a solar-thermal system employing seasonal storage for providing the majority of space heating and domestic hot water heating needs to a single-family house in a cold climate. Solar Energy 191 (2019) 57–69

Belussi, L., Barozzi, B., Bellazzi, A., Danza, L., Devitofrancesco, A., Fanciulli, C., Ghellere, M., Guazzi, G., Meroni, I., Salamone, F., Scamoni, F., Scrosati, C. (2019). A review of performance of zero energy buildings and energy efficiency solutions. Journal of Building Engineering 25 (2019) 100772

Besheer, A., Smyth, M., Zacharopoulos, A., Mondol, J., Pugsley, A. (2016). Review on recent approaches for hybrid PV/T solar technology. International Journal of Energy Research. DOI: 10.1002/er.3567

Bilardo, M., Fraisse, G., Pailha, M., Fabrizio, E. (2019). Modelling and performance analysis of a new concept of integral collector storage (ICS) with phase change material. Solar Energy 183 (2019) 425–440

Borello, D., Corsini, A., Delibra, G., Evangelisti, S., Micangeli, A. (2012). Experimental and computational investigation of a new solar integrated collector storage system. Applied Energy 97 (2012) 982–989

Boreyko, J. & Chen, C. (2013). Vapor chambers with jumping-drop liquid return from superhydrophobic condensers. International Journal of Heat and Mass Transfer 61 (2013) 409–418

Bosch (2010). High performance – Stable yields. Bosch Solar Cell M 2BB. [Last accessed: 10 September 2016]. Arnstadt, Germany: Bosch Solar Energy AG. Available at: <http://www.bosch-solarenergy.com>.

Buonomano, A., Calise, F., Palombo, A., Vicidomini, M. (2016). BIPVT systems for residential applications: An energy and economic analysis for European climates. Applied Energy 184 (2016) 1411–1431

Calise, F., d'Accadia, M, Figaj, R., Vanoli, L., (2016). A novel solar-assisted heat pump driven by photovoltaic/thermal collectors: Dynamic simulation and thermoeconomic optimization. Energy 95, 346-66

Chaabane, M., Mhiri, H., Bournot, P. (2014). Thermal performance of an integrated collector storage solar water heater (ICSSWH) with phase change materials (PCM). Energy Conversion and Management 78 (2014) 897–903.

COST Action TU1205 (2015). Overview of BISTS state of the art, models and applications. ISBN: 978-9963-697-16-8. Cyprus University of Technology / European Union Horizon 2020.

Das, D., Kalita, P., Roy, O. (2018). Flat plate hybrid photovoltaic- thermal (PV/T) system: A review on design and development. Renewable and Sustainable Energy Reviews 84 (2018) 111–130

De Beijer, H. (1998). Product development in solar water heating. Renewable Energy 5 (1998) 201-204

Deng, J., O'Donovan, T., Tian, Z., King, J., Speake, S. (2019). Thermal performance predictions and tests of a novel type of flat plate solar thermal collectors by integrating with a freeze tolerance solution. Energy Conversion and Management 198 (2019) 111784

DGS - Deutsche Gesellshaft fur Sonnenenergie (2008). Planning and Installing Photovoltaic Systems - A guide for installers, architects and engineers. 2nd ed. London: Earthscan. ISBN-13: 978-1-84407-442-6

Drosou, V., Tsekouras, P., Oikonomou, T., Kosmopoulos, P., Karytsas, C. (2014). The HIGH-COMBI project: High solar fraction heating and cooling systems with combination of innovative components and methods. Renewable and Sustainable Energy Reviews 29 (2014) 463–472

Dupeyrat, P., Menezo, C., Rommel, M., Henning, H. (2011). Efficient single glazed flat plate photovoltaic-thermal hybrid collector for domestic hot water systems. Solar Energy 85, 1457-68

Eames, P. and Griffiths, P. (2006). Thermal behaviour of integrated solar collector/storage unit with 65C phase change material. Energy Conversion and Management 47 (2006) 3611–3618

Faiman, D., Hazan, H. and Laufer, I. (2001). Reducing the Heat Loss at Night from Solar Water Heaters of the Integrated Collector-Storage Variety. Solar Energy, 71 (2) 87-93

Fuentes, M., Vivar, M., Casab, J., Aguilera, J. (2018). An experimental comparison between commercial hybrid PV-T and simple PV systems intended for BIPV. Renewable and Sustainable Energy Reviews 93 (2018) 110–120

Garnier, C., Currie, J., Muneer,T. (2009). Integrated collector storage solar water heater: Temperature stratification. Applied Energy 86 (2009) 1465–1469

Good, C., Andresen, I., Hestnes, A. (2015). Solar energy for net zero energy buildings – A comparison between solar thermal, PV and photovoltaic–thermal (PV/T) systems. Solar Energy 122, 986–96

Guarracino, I., Freeman, J., Ramos, A., Kalogirou, S., Ekins-Daukes, N., Markides, C. (2019). Systematic testing of hybrid PV-thermal (PVT) solar collectors in steady-state and dynamic outdoor conditions. Applied Energy 240 (2019) 1014–1030

Harmim, A., Boukar, M., Amar, M., Haida, A. (2019). Simulation and experimentation of an integrated collector storage solar water heater designed for integration into building façade. Energy 166 (2019) 59-71

IEA – International Energy Agency (2018). Key World Energy Statistics 2018. Paris, France: IEA.

IEA/UN - International Energy Agency and the United Nations Environment Programme (2018). 2018 Global Status Report: towards a zero-emission, efficient and resilient buildings and construction sector. Paris, France: IEA for the Global Alliance for Buildings and Construction (GlobalABC). ISBN: 978-92-807-3729-5.

Kalogirou, S. (2009). Solar energy engineering. London: Academic Press (Elsevier) ISBN 13: 978-0-12-374501-9

Kats, G., Seal, A. (2012). Buildings as Batteries: The Rise of 'Virtual Storage'. The Electricity Journal 25 (10) 59-70 http://dx.doi.org/10.1016/j.tej.2012.11.004

Krauter, S. (2004). Development of an integrated solar home system. Solar Energy Materials & Solar Cells 82 (2004) 119–130

Li, S., Zhang, Y., Zhang, K., Li, X., Li, Y., Zhang, X. (2013). Study on performance of storage tanks in solar water heater system in charge and discharge progress (SHC 2013, International Conference on Solar Heating and Cooling for Buildings and Industry). Energy Procedia 48 (2014) 384–393 doi: 10.1016/j.egypro.2014.02.045

Li, X., Lin, A., Young, C., Dai, Y., Wang, C. (2019). Energetic and economic evaluation of hybrid solar energy systems in a residential net-zero energy building. Applied Energy 254 (2019) 113709

Mehdaoui, F., Hazami, M., Messaouda, A., Guizani, A. (2019). Performance analysis of two types of Solar Heating Systems used in buildings under typical North-African climate (Tunisia). Applied Thermal Engineering (AIP) https://doi.org/10.1016/j.applthermaleng.2019.114203

Michael, J., Iniyan, S., Goic, R. (2015). Flat plate solar photovoltaic–thermal (PV/T) systems. Renewable & Sustainable Energy Reviews 51, 62–88

Mohamad, A. (1997). Integrated Solar Collector-Storage Tank System with Thermal Diode. Solar Energy 61 (3) 211-218

Muhumuza, R., Zacharopoulos, A., Mondol, J., Smyth, M. (2019a). Experimental study of heat retention performance of thermal diode Integrated Collector Storage Solar Water Heater (ICSSWH) configurations. Sustainable Energy Technologies and Assessments 34 (2019) 214–219

Muhumuza, R., Zacharopoulos, A., Mondol, J., Smyth, M., Pugsley, A., Giuzio, G., Kurmis, D. (2019b). Experimental investigation of horizontally operating thermal diode solar water heaters with differing absorber materials under simulated conditions. Renewable Energy, Volume 138, August 2019, Pages 1051-1064

Muhumuza, R., Zacharopoulos, A., Mondol, J., Smyth, M., Pugsley, A., McGee, J. (2020). Simulation and experimental validation of solar radiation distribution on the absorber of a line-axis asymmetric compound parabolic concentrator. Solar Energy 198 (2020) 36-52. https://doi.org/10.1016/j.solener.2020.01.033.

NASA - National Aeronautics and Space Administration (2019). Data Access Viewer for Prediction of Worldwide Energy Resource (POWER) Project funded through the NASA Earth Science/Applied Science Program. Hampton, USA: Langley Research Center (LaRC). Available at: < https://power.larc.nasa.gov/data-access-viewer/ > [Last accessed: 07/10/19].

O'Hegarty, R., Kinnane, O., McCormack, S. (2014). A Case for façade located solar thermal collectors. (International Conference on Solar Heating and Cooling for Buildings and Industry, SHC 2014). Energy Procedia 70 (2015) 103–110 doi: 10.1016/j.egypro.2015.02.104

Pugsley, A., Mondol, J., Smyth, M., Zacharopoulos, A., Di Mattia, L. (2016). Experimental characterisation of a flat panel integrated collector-storage solar water heater featuring a photovoltaic absorber and a planar liquid-vapour thermal diode. Proceedings of 11th ISES EuroSun Conference: Palma (Mallorca), Spain from 11 to 14 October 2016. Martinez, V. & Gonzalez, J. (eds.).

Pugsley, A. (2017). Theoretical and experimental analysis of a novel flat photovoltaic-thermal solar water heater with integrated energy storage via a planar liquid-vapour thermal diode. Ulster University PhD Thesis (uk.bl.ethos.713462) published July 2017.

Pugsley, A., Zacharopoulos, A., Mondol, J., Smyth, M. (2019). Theoretical and experimental analysis of a horizontal Planar Liquid-Vapour Thermal Diode (PLVTD). International Journal of Heat and Mass Transfer 144 (2019) 11866

Pugsley, A., Zacharopoulos, A., Mondol, J., Smyth, M. (2020). Vertical Planar Liquid-Vapour Thermal Diodes (PLVTD) and their application in building façade energy systems. Applied Thermal Engineering (submitted for publication 01/2020, under review)

Qu, M., Chen, J., Nie, L., Li, F., Yu, Q., Wang, T. (2016). Experimental study on the operating characteristics of a novel photovoltaic/thermal integrated dual-source heat pump water heating system. Applied Thermal Engineering 94, 819–26

Quinlan, P. (2010). The Development of a Novel Integrated Collector Storage Solar Water Heater (ICSSWH) Using Phase Change Materials and Partial Evacuation. PhD Thesis, University of Ulster.

Rhee, J., Campbell, A. Mariadass, A., Morhous, B. (2010). Temperature stratification from thermal diodes in solar hot water storage tank. Solar Energy 84 (2010) 507–511

Santbergen, R., Rindt, C., Zondag, H., Van Zolingen, R. (2010). Detailed analysis of the energy yield of systems with covered sheet-and-tube PVT collectors. Solar Energy 84, 867–78.

Saretta, E., Bonomo, P., Frontini, F. (2020). A calculation method for the BIPV potential of Swiss façades at LOD2.5 in urban areas: A case from Ticino region. Solar Energy 195 (2020) 150–165

Schmidt, C. and Goetzberger, A. (1990). Single-Tube Integrated Collector Storage Systems with Transparent Insulation and Involute Reflector. Solar Energy 45 (2) 93-100

Singh, R., Lazarus, I., Souliotis, M. (2016). Recent developments in integrated collector storage (ICS) solar water heaters: A review. Renewable & Sustainable Energy Reviews 54, 270-98

Smyth, M., Eames, P., Norton, B. (1999). A comparative performance rating for an integrated solar collector/storage vessel with inner sleeves to increase heat retention. Solar Energy 66 (4) 291–303.

Smyth, M., Eames, P., Norton, B. (2003). Heat Retaining Integrated Collector/Storage Solar Water Heaters. Solar Energy 75 (2003) 27-34

Smyth, M., McGarrigle, P., Eames, P., Norton, B. (2005). Experimental comparison of alternative convection suppression arrangements for concentrating integral collector storage solar water heaters. Solar Energy 78 (2005) 223–233

Smyth, M., Eames, P. and Norton, B. (2006). Integrated Collector Storage Solar Water Heaters. Renewable and Sustainable Energy Review 10 (6) 503-538

Smyth, M. (2015a). A solar water heater. Patent WO2010052010 held by Ulster University.

Smyth, M., Besheer, A., Zacharopoulos, A., Mondol, J., Pugsley, A., Novaes, M. (2015b). Experimental evaluation of a Hybrid Photovoltaic/Solar Thermal (HyPV/T) Façade Module. Proceedings EURO ELECS Conference 21-23 July 2015, Guimarães, Portugal.

Smyth, M., Quinlan, P., Mondol, J., Zacharopoulos, A., McLarnon, D., Pugsley, A. (2017). The evolutionary thermal performance & development of a novel thermal diode pre-heat solar water heater under simulated heat flux conditions. Renewable Energy 113 (2017) 1160-1167

Smyth, M., Quinlan, P., Mondol, J., Zacharopoulos, A., McLarnon, D., Pugsley, A. (2018). The experimental evaluation and improvements of a novel thermal diode pre-heat solar water heater under simulated solar conditions. Renewable Energy 121 (2018) 116-122

Smyth, M., Pugsley, A., Hanna, G., Zacharopoulos, A., Besheer, A., Savvides, A. (2019). Experimental performance characterisation of a Hybrid Photovoltaic/Solar Thermal Façade module compared to a flat Integrated Collector Storage Solar Water Heater module. Renewable Energy 137 (2019) 137-143

Sopian, K., Syahri, M., Abdullah, S., Othman, M.,Yatim, B. (2004). Performance of a non-metallic unglazed solar water heater with integrated storage system. Renewable Energy 29 (2004) 1421–1430

Souliotis, M., Quinlan, P., Smyth, M., Tripanagnostopoulos, Y., Zacharopoulos, A., Ramirez, M., Yianoulis, P. (2011). Heat retaining integrated collector storage solar water heater with asymmetric CPC reflector. Solar Energy 85 (2011) 2474–87

Souliotis, M., Chemisana, D., Caouris, Y., Tripanagnostopoulos, Y. (2013). Experimental study of integrated collector storage solar water heaters. Renewable Energy 50 (2013) 1083-1094

Souliotis, M., Papaefthimiou, S., Caouris, Y., Zacharopoulos, A., Quinlan, P., Smyth, M. (2017). Integrated collector storage solar water heater under partial vacuum. Energy 139 (2017) 991-1002

Stackhouse, P., Zhang, T., Westberg, D., Barnett, A., Bristow, T., Macpherson, B., Hoell, J. (2018). POWER Release 8.0.1 (with GIS Applications) Methodology, Data Parameters, Sources, & Validation. Data Version 8.0.1. Web Site Version 1.1.0. Hampton, USA: NASA LaRC, Langley Research Center.

Sultan, S., Efzan, E. (2018). Review on recent Photovoltaic/Thermal (PV/T) technology advances and applications. Solar Energy 173 (2018) 939–954

Tian, M., Yu, X., Su, Y., Zheng, H., Riffat, S. (2019). A study on incorporation of transpired solar collector in a novel multifunctional PV/Thermal/Daylighting (PV/T/D) panel. Solar Energy 165 (2018) 90–99

Tripanagnostopoulos, Y., Souliotis, M., Nousia, T. (2002). CPC type collector storage systems. Solar Energy 72 (4) 327-350

Tripanagnostopoulos, Y., Souliotis, M. (2006). ICS Solar Systems with Two Water Tanks. Renewable Energy 29 (1) 13-38

Twidell, J. & Weir, T. (2006). Renewable Energy Resources (2nd ed.) London: Taylor Francis. ISBN13:9-78-0-419-25330-3

Yang, T., Athienitis, A. (2016). A review of research and developments of building-integrated photovoltaic/thermal (BIPV/T) systems. Renewable and Sustainable Energy Reviews 66 (2016) 886–912

Ziapour, B., Palideh, V., Mohammadnia, A. (2014). Study of an improved integrated collector-storage solar water heater combined with the photovoltaic cells. Energy Conversion and Management 86 (2014) 587–594.

Zondag, H. (2008). Flat-plate PV–thermal collectors and systems: a review. Renewable & Sustainable Energy Reviews 12, 891–959.